CHAPTER 4

Readily prepared peroxidomolybdenum based homogeneous and heterogeneous catalysts for selective oxidation of sulfides in aqueous medium

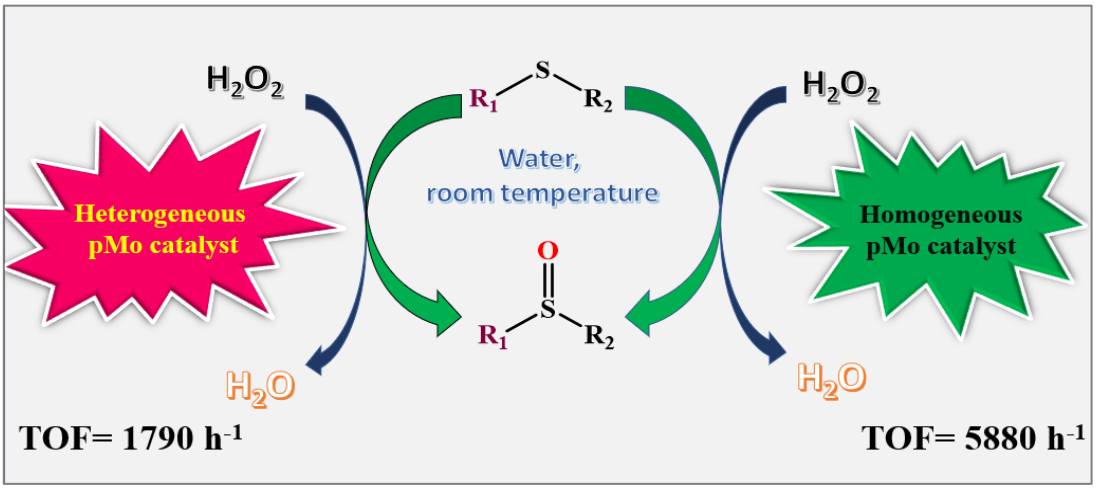

4.1 Introduction

In continuation of our efforts to develop simple and sustainable routes to accomplish selective sulfoxidation in aqueous medium, in the present work we have attempted to explore the scope of generating new peroxidomolybdenum (**pMo**) based catalysts using water soluble polymers (WSP) as supports. Importance of peroxido compounds of molybdenum as versatile catalysts or oxidant in a variety of organic oxidations including several industrial processes has been adequately highlighted in the literature as well as in the introductory Chapter. We have envisaged that the combination of WSP support with a catalytically active **pMo** species would add advantages of polymeric reagent (stability and phase homogeneity to the catalyst and oxidant, for instance) to the inherent oxidant ability of the **pMo** species to afford water compatible and recoverable catalysts usable in aqueous medium.

Albeit a homogeneous catalyst usually exhibits superior activity and selectivity *vis-à-vis* its heterogeneous counterpart, nevertheless, due to the ever increasing emphasis on cleaner and sustainable chemical processes development of heterogeneous selective oxidation catalysts that support green and energy efficient oxidation reactions has assumed tremendous importance [1-3]. In recent years, natural polymers such as cellulose, chitin and chitosan have been attracting considerable attention as promising green support materials for heterogenization of metal catalysts [4-8]. The unique features of chitosan, one of the most abundant biopolymers in nature [9-14], such as their non-toxicity, biodegradability, biocompatibility and easy accessibility make it vastly attractive for a wide variety of potential applications in areas ranging from therapeutics, cosmetics, food processing to environmental applications [5-14].

There has been plethora of reports demonstrating heterogenized chitosan metal complexes as catalysts in diverse organic transformations such as hydrogenation [15-17], condensation [18,19], water splitting reaction [20,21], coupling reaction [22-24], polymerization [25,26], hydroxylation [27,28], Suzuki and Heck reactions [29-33] etc. However, we have so far come across only two reports dealing with the application of peroxidometal derivative supported on chitosan as oxidation catalysts [34,35].

Among the limited reports available on water-based metal-catalyzed sulfide oxidation processes, studies devoted to water compatible heterogeneous systems are still rare [36-43]. As mentioned in preceding Chapter, despite of the development of scores of

promising methodologies for selective sulfide oxidation with H_2O_2 using both homogeneous and heterogeneous transition metal catalysts reported in recent years, there still remains plenty of opportunities to design new alternative catalysts which can perform optimally in safer reaction media under mild condition, as some of the available methodologies still rely upon volatile and toxic organic solvents [41,44-57].

In this chapter we describe the preparation and characterization of a heretofore unreported chitosan immobilized peroxidomolybdenum complex (**PMoCh**), which displayed excellent selectivity and efficiency as a water tolerant heterogeneous catalyst, for the oxidation of a diverse range of thioethers by H_2O_2 in water, under eco-friendly reaction conditions. In addition, development of a new water based homogeneous catalytic protocol for H_2O_2 mediated selective sulfide oxidation using diperoxidomolybdenum(VI) species anchored to linear WSP resins of the type, $[MoO(O_2)_2(sulfonate)]$–PS [PS = poly(sodium vinyl sulfonate)] (**PSMo**) or $[Mo_2O_2(O_2)_4(carboxylate)]$–PA [PA = poly(sodium acrylate)] (**PAMo**) as recyclable catalysts is also presented herein. Pertinent here is to mention that, synthesis and characterization of these water soluble macro complexes and their unique biochemical activity have been reported previously from our laboratory [58,59].

The work presented in this chapter has been distributed over two sections.

4.2 Section A:

A new chitosan supported Mo(VI) complex as heterogeneous catalyst for selective oxidation of thioethers in water

4.2.1 Experimental section

4.2.1.1 Synthesis of chitosan supported dioxidomonoperoxidomolybdenum(VI) catalyst (PMoCh)

Molybdic acid (1 g, 6.25 mmol) was dissolved in 7 mL of 30% H_2O_2(62.5 mmol) at room temperature. The pH of the clear solution at this stage was recorded to be *ca.* 1. The solution pH was then slowly raised to *ca.* 7 by dropwise addition of concentrated sodium hydroxide (*ca.* 8 M) with constant stirring. Maintaining the temperature of the reaction mixture below 4^0C in an ice bath, 1.0 g of Chitosan (Ch) was added to it with constant stirring. The reaction mixture was kept as such for 24 h. The resulting mixture was then filtered and the yellow residue was repeatedly washed with pre-cooled acetone. The obtained product was dried in vacuo over concentrated sulfuric acid.

4.2.1.2 Elemental analysis

Quantitative determination of molybdenum, peroxido, carbon, hydrogen, nitrogen and sodium were accomplished by methods described in Chapter 2. The analytical data of the compounds are presented in **Table 4.1**.

4.2.1.3 Physical and spectroscopic measurements

The compound was characterized according to the described methods in Chapter 2, with the help of spectroscopic measurements, thermogravimetric analysis as well EDX analysis. **Table 4.3** summarizes the structurally significant IR and Raman bands along with their assignments. Solid state ^{13}C NMR chemical shift values of the complex are represented in the **Table 4.4** and spectra are presented in **Fig. 4.8**. TGA of the complex is represented in the **Fig. 4.9-4.10**.

4.2.1.4 Computational details

Density functional theory (DFT) calculation has been performed using DMol^3 package [60]. The van der Waals interactions have been taken into consideration while performing theoretical calculations, as polymeric structures bind through these interactions. Dispersive forces, or van der Waals forces, result from the interaction between fluctuating multipoles without requiring the overlap of electron densities [61] Therefore, we have used dispersion corrected density functional theory (DFT-D) for geometry optimization and frequency analysis. Local density models, such as the VWN

(Vosko, Wilk and Nusair) [62] functional, are simple and computationally efficient. DFT-D approaches to treat vdW interactions employed using the Ortmann, Bechstedt and Schmidt [63] (OBS) correction to VWN. We have used DNP (double numerical plus polarization) [60] basis set for our calculation. For the heavy metal Mo, the valence electrons are described by double numerical basis set with polarization function and the core electrons are described with local pseudo-potential (VPSR) which accounts for the scalar relativistic effect expected to be significant for heavy metal elements [64,65]. The geometry has been fully relaxed and positive vibrational frequency confirms the complex to be at energy minimum.

4.2.1.5 General procedure for catalytic oxidation of sulfides to sulfoxides

In a typical procedure, the oxidation reaction was carried out by placing organic substrate (5mmol), catalyst **PMoCh** (1.4 mg, containing 0.0025 mmol of Mo), 30% H_2O_2 (2.26 mL, 20 mmol) in 5 mL of solvent (water or methanol) in a round bottom flask. The molar ratio of catalyst Mo: substrate was maintained at 1:2000 and substrate:H_2O_2 at 1:4. The reaction was conducted at ambient temperature under magnetic stirring. The progress of the reaction was monitored by thin layer chromatography (TLC) and GC. After completion of the reaction, the heterogeneous catalyst was separated by filtration, followed by washing with acetone. The oxidized product along with unreacted organic substrates were extracted with diethyl ether, dried over anhydrous sodium sulfate and distilled under reduced pressure to remove excess diethyl ether. The product was then purified by column chromatography on silica gel with ethyl acetate-hexane (1:9 v/v) as the eluent. The product obtained was characterized by IR, ^{1}H NMR, ^{13}C NMR spectroscopy and melting point determination (for solid products) (**Appendix I**).

4.2.1.6 Regeneration of the catalyst

The recyclability of the catalyst was tested employing methyl phenyl sulfide as the substrate, in reactions conducted independently in aqueous medium as well as in methanol. After completion of the reaction in each run, the solid catalyst was separated from the spent reaction mixture by filtration, as mentioned above. The recovered catalyst was washed with acetone and dried *in vacuo* over concentrated sulfuric acid. The dried catalyst was then placed in the next fresh batch of reaction containing 30% H_2O_2 (2.26 mL, 20 mmol), substrate (5 mmol) and solvent (H_2O or MeOH, 5 mL). The reaction was allowed

to proceed under optimized condition in the same manner as that of the first run. The progress of the reaction was monitored by thin layer chromatography (TLC) and GC.

In an alternative methodology, the used catalyst could also be recycled simply by charging the spent reaction mixture remaining in the reaction vessel after separating the organic reaction product, with a fresh lot of H_2O_2, sulfide and then repeating the experiment as mentioned above. Each of the procedures was performed under optimized reaction condition for six reaction cycles.

4.2.2 Results and Discussion

4.2.2.1 Catalyst preparation and characterization

The synthesis of the peroxidomolybdenum catalyst **PMoCh**, immobilized on chitosan was achieved by establishing a reasonably straightforward methodology, involving the reaction of in-situ generated peroxidomolybdenum species with chitosan in water under mild reaction condition. As chitosan is known to be water soluble under acidic conditions, the pH of the reaction medium was strategically maintained above 7 in order to obtain the solid catalyst in a water insoluble form. Maintenance of reaction temperature at < 4 ^{0}C and contact time of 24 h was also observed to be equally important for the successful synthesis of the catalyst. The catalyst is non-hygroscopic and remains stable for weeks without change in its catalytic activity.

For characterization of the newly synthesized catalyst, combinations of a host of spectroscopic and other physicochemical techniques have been made use of, apart from elemental analysis. From the elemental analysis data of **PMoCh**, the ratio of Mo:O^{2-} content was found to be 1:1, in conformity with the presence of **pMo** moieties in the catalyst in their monoperoxido form. The Mo loading on chitosan, determined from the Mo content obtained from elemental analysis, EDX analysis and inductively coupled plasma optical emission spectrophotometric analysis (ICP-OES) was found to be 1.77 mmol g^{-1} of the polymer (**Table 4.1**). The diamagnetic nature of the **pMo** compound was evident from the magnetic susceptibility measurement, in agreement with the occurrence of Mo in its + 6 oxidation state.

Table 4.1 Analytical data for the synthesized complex **PMoCh**

	% Found from elemental analysis (% obtained from EDX spectra)					
Complex	C	H	N	Mo	O_2^{2-}	Molybdenum loading[a] (mmol g^{-1} of polymer)
PMoCh	32.30	4.71	6.13	17.02	6.21	1.77
	(31.54)	--	(5.96)	17.10[b]	--	
	--	--	--	(17.16)	--	

[a] Molybdenum loading = $\frac{\text{Observed metal \% } \times 10}{\text{Atomic weight of metal}}$

[b] Determined by ICP-OES

4.2.2.2 Scanning electron microscopy (SEM) and energy dispersive X-ray (EDX) analysis

The surface topography of chitosan before and after metal complexation was investigated by scanning electron microscope. The SEM images of pure chitosan (Ch) displayed cavities at its different imaging ranges as seen in **Fig. 4.1(a)** and **4.1(c).** The SEM micrograph of the Mo-Chitosan complex **PMoCh**, on the other hand, showed a relatively smooth surface. The considerable morphological changes on the surface of chitosan observed after metal anchoring compared to the pure chitosan, clearly indicated chemical modification of the polymer [**Fig. 4.1(b)** and **4.1(d)**]. The observed changes of molybdenum anchored chitosan, **PMoCh**, may be ascribed to anchoring of metal ions *via* amino groups of chitosan. Support for such an observation comes from previous reports which demonstrated that strong complexation of metal ions to the amino functions of chitosan resulted in smooth surface morphology of the metal anchored chitosan [66-68].

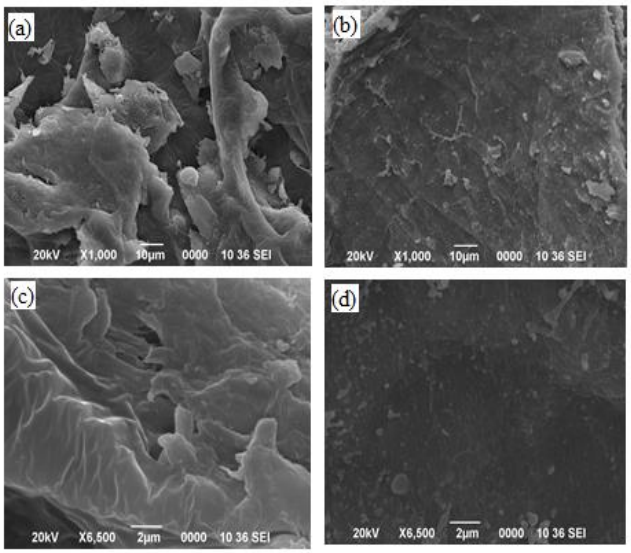

Fig. 4.1 Scanning electron micrographs of chitosan **1**(**a**), (**c**) and **PMoCh 1**(**b**), (**d**).

The Energy-dispersive X-ray (EDX) spectroscopic analysis data provided evidence for the presence of Mo in the compound, apart from the C, N and O atoms (**Fig. 4.2**). The EDX analysis, which gives *in situ* chemical analysis of the bulk, was carried out by focusing multiple regions over the surface of the polymeric compound. The results derived from EDX analysis and ICP-OES analysis were in good agreement with elemental analysis values.

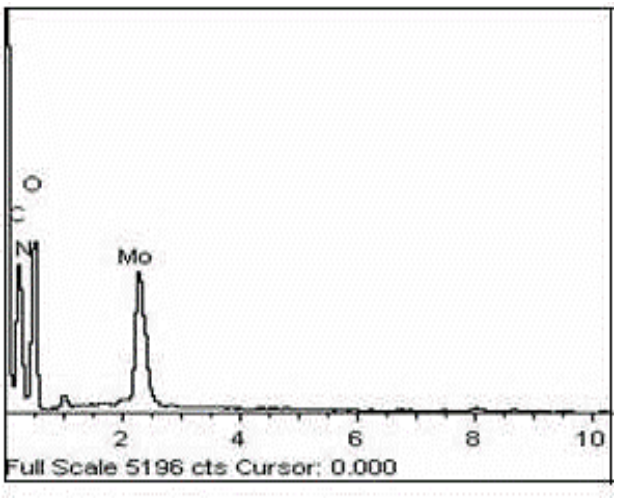

Fig. 4.2 EDX spectrum of **PMoCh**.

4.2.2.3 X-ray diffraction studies

The X-ray diffraction pattern of pure chitosan (**Ch**) and peroxidomolybdate incorporated chitosan (**PMoCh**) are illustrated in **Fig. 4.3**. In the XRD spectrum, chitosan shows two typical broad peaks along with a sharp peak due to its semi crystalline nature at 2θ of 12.7, 19.9 and 26.7 respectively [66,69-71]. Complexation of metal ions with biopolymers in general, is known to induce changes in crystallinity of the polymer [69-71]. In case of the catalyst **PMoCh**, the XRD patterns revealed a decrease in intensity of the characteristic peaks of chitosan with concomitant appearance of several new diffraction peaks, indicative of formation of a new crystalline phase. The decrease in intensity of the chitosan peaks is likely to be owing to the disruption of inter polymer hydrogen bonds as a result of binding of the metal ions to chitosan *via* $–NH_2$ or -OH groups [69-71]. The diffractogram of **PMoCh** complex displayed new major peaks at 2θ values 14.6, 15.8, 24.4, 26.7, 27.8, 29.0 and 31.90. These values are close to the peak values observed for monoperoxido molybdate species (PDF 41-359) which were assigned to (200), (101), (110),

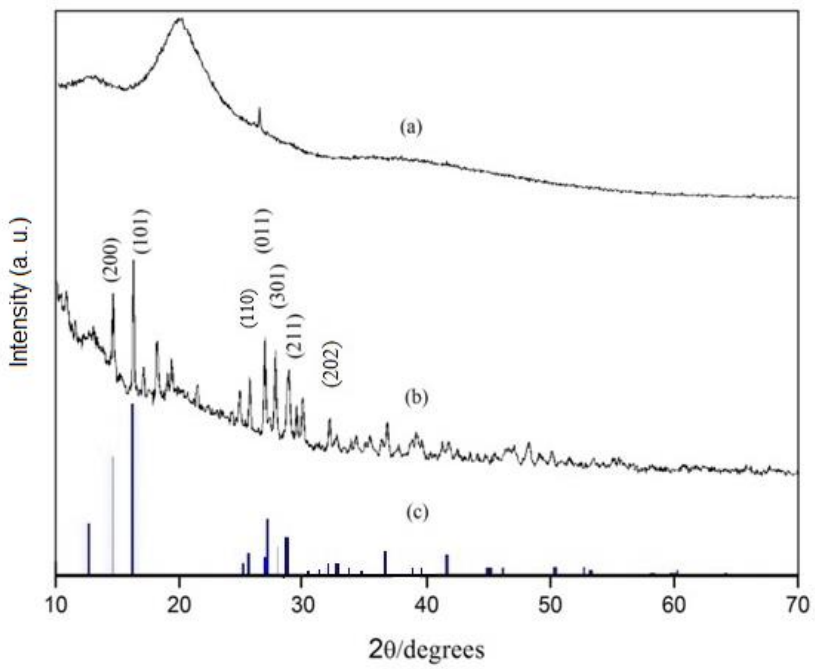

Fig. 4.3 Powder X-ray diffraction pattern of (a) **Ch**, (b) **PMoCh** and (c) reference powder X-ray diffraction pattern of H_2MoO_5 (JCPDS card number 41-359).

(011), (301), (211) and (202) planes, respectively. That the monoperoxido molybdenum moieties are anchored to the polymer to afford the chitosan supported **PMoCh** catalyst has thus been confirmed.

4.2.2.4 BET analysis

The specific surface area of compound, **PMoCh** and pure chitosan (**ch**) were measured by employing BET analysis with the nitrogen adsorption method and the pore volume was obtained by BJH model [72,73]. The adsorption-desorption isotherm of the catalyst (**Fig. 4.4**) showed typical type II adsorption of an IUPAC standard on particles which have macropores or nonpores [74,75]. The textural properties of neat chitosan and Mo incorporated chitosan catalyst are presented in **Table 4.2**. The results showed that after anchoring of **pMo** moieties the surface area of chitosan (3.0 m^2/g) as well as total pore volume (0.05 mL/g) increased to 11.4 m^2/g and 0.56 mL/g, respectively. The average pore diameter of chitosan did not show any significant change after complexation. The increase in surface area and total volume of the catalyst relative to pure chitosan provided clear indication of complexation of metal with the polymer.

Table 4.2 BET surface area, pore volume and average pore diameter of pure polymer (**ch**) and compound **PMoCh**

Adsorbents	Chitosan (**Ch**)	**PMoCh**
BET surface areas (m^2/g)	3.0	11.4
Pore volume (mL/g)	0.05	0.56
Average pore diameter (Å)	32.0	32.0

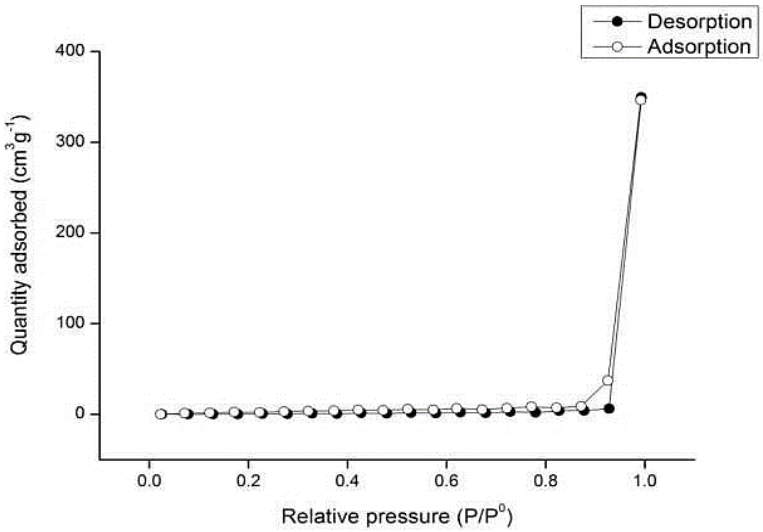

Fig. 4.4 BET N_2-adsorption-desorption isotherm of **PMoCh**.

4.2.2.5 FTIR and Raman spectral studies

The FT-IR spectra of chitosan (**Ch**) and chitosan anchored peroxidomolybdenum catalyst (**PMoCh**) are shown in the **Fig. 4.5** and the corresponding significant spectral data are summarized in **Table 4.3**. The intense broad band in the spectrum of the pristine chitosan, centered at 3434 cm^{-1} has been ascribed to the stretching vibration of $-NH_2$ and -OH groups which usually overlap and occur in the equivalent region [14,35,68,76-83]. In the spectrum of complex **PMoCh**, observance of the band at a lower frequency of 3415 cm^{-1}, indicated the participation of amine or hydroxyl, or both of these groups of chitosan in metal co-ordination [35,68,69,71].

Further evidence in support of the co-ordination of the metal *via* secondary –OH and primary amine groups has been obtained from the distinct shift of the bands occurring at 1089 cm^{-1} (secondary -OH) and 1592 cm^{-1} (N-H bending) in the free polymer to lower values of 1066 and 1561 cm^{-1}, respectively in the spectrum of the complex **PMoCh** [14, 35,76-83]. The band at 1038 cm^{-1} of chitosan remained unaffected in **PMoCh** implying that the primary -OH group is not involved in complexation [14,76-83]. The typical band at 1646 cm^{-1} (C–O stretching along with N–H deformation mode, amide I) in the spectrum of chitosan remained practically unaltered in its position in the spectrum of the catalyst demonstrating that the group was not involved in metal co-ordination [76-83]. The spectrum of the complex also displayed other characteristic bands of chitosan such as

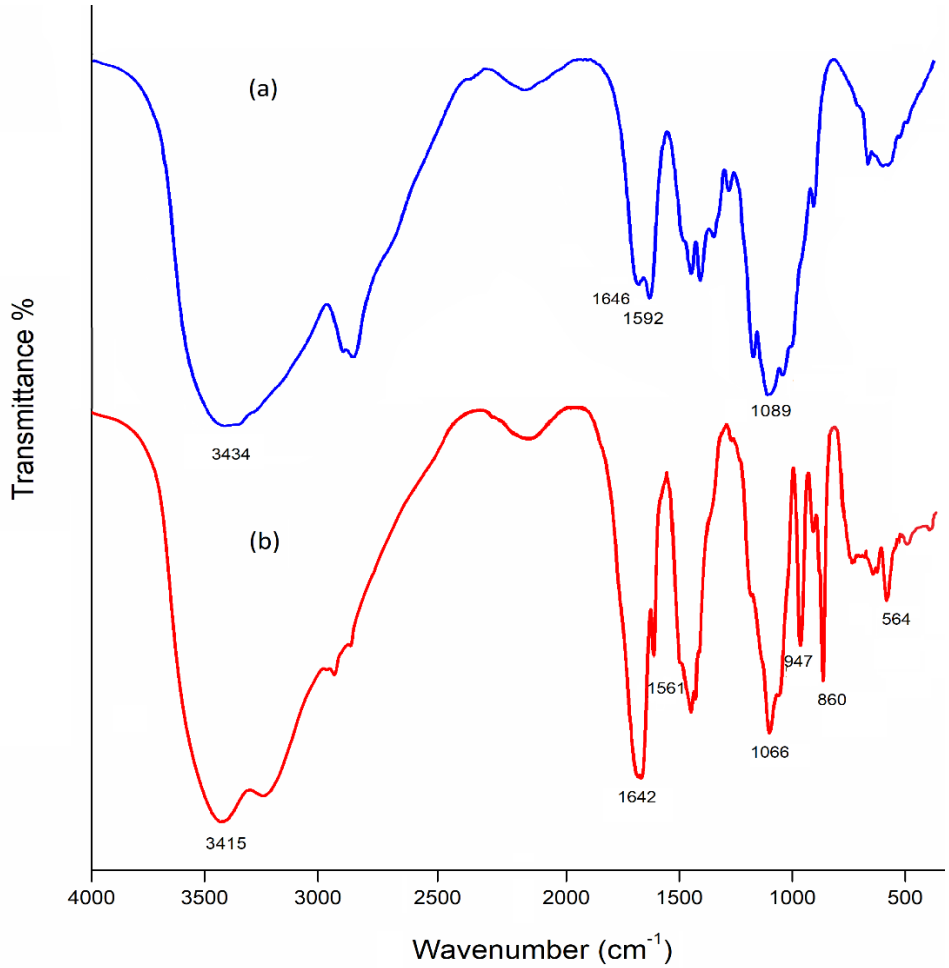

Fig. 4.5. IR spectra of (a) Chitosan and (b) catalyst **PMoCh**.

β-(1→4) glycoside C-O-C bridge bands at *ca.* 1160 and 894 cm^{-1}, C-H stretching vibrations at the expected region of 2927 and 2855 cm^{-1} indicating that the metal complex successfully anchored to chitosan [35,76-83].

Table 4.3 Experimental and theoretical infrared (IR) and Raman (R) spectral data (cm^{-1}) for **PMoCh** complex

Assignment			**PMoCh**	Assignment			**PMoCh**
$\nu(NH_2 + OH)$	IR	Exp.	3415	$\nu(Mo{=}O)$	IR	Exp.	947
		Calc.	3403			Calc.	939
ν(C-O, secondary OH)	IR	Exp.	1066		R	Exp.	948
		Calc.	1079			Calc.	958
	R	Exp.	1059	$\nu_{asym}(Mo\text{-}O_2)$	IR	Exp.	629
		Calc.	1058			Calc.	621
Amide I	IR	Exp.	1642		R	Exp.	610
[$\nu(CO)+\delta(NH)$]		Calc.	1623			Calc.	614
	R	Exp.	1638	$\nu_{sym}(Mo\text{-}O_2)$	IR	Exp.	536
		Calc.	1599			Calc.	541
δ(N-H)	IR	Exp.	1561		R	Exp.	523
		Calc.	1556			Calc.	530
	R	Exp.	1551	ν(Mo-O)	IR	Exp.	465
		Calc.	1585			Calc.	456
ν(C-O-C)	IR	Exp.	894		R	Exp.	460
		Calc.	889			Calc.	456
	R	Exp.	907	ν(O-O)	IR	Exp.	860
		Calc.	905			Calc.	863
					R	Exp.	830
						Calc.	826

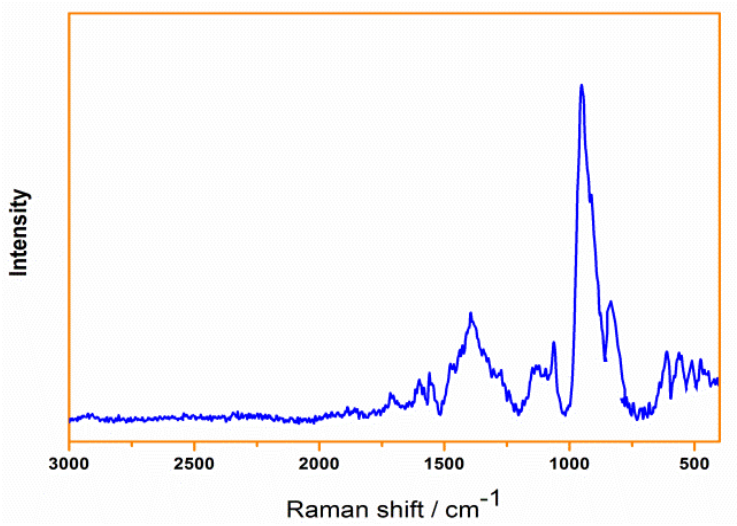

Fig. 4.6. Raman spectrum of **PMoCh**.

The band at 564 cm^{-1} ascribed to Mo-N bond further signifies the complexation of metal with chitosan through $–NH_2$ group [35,84,76-83]. The 465 cm^{-1} band in the complex is due to Mo-O bond in the complex [35,84,76-83]. The presence of molybdenum peroxido and oxido groups of the $[Mo(O)_2O_2]$ moiety in the complex was confirmed by the occurrence of typical bands at *ca.* 860, 947, 629 and 536 cm^{-1} corresponding to ν(O-O), ν(Mo = O), $\nu_{asym}(Mo\text{-}O_2)$ and $\nu_{sym}(Mo\text{-}O_2)$ was supported by the complementary Raman spectrum (**Fig. 4.6**) which displayed bands at 948, 830, 907, 610, 523 and 460 cm^{-1} corresponding to ν(Mo=O), ν(O-O), ν(C-O-C), $\nu_{asym}(Mo\text{-}O_2)$, $\nu_{sym}(Mo\text{-}O_2)$ and ν(Mo-O) vibrations, respectively [46,85,86]. The spectrum also shows two peaks at 1638 and 1551 cm^{-1} attributable to amide I and NH deformation modes, respectively [87].

4.2.2.6 Electronic spectral studies

The diffuse reflectance UV-visible spectrum of **PMoCh** is given in **Fig. 4.7**. The spectrum shows two broad bands with maxima at 275 and 364 nm. The weak intensity absorbance at 364 nm is characteristic of monoperoxidomolybdate(VI) species due to peroxido to metal LMCT transition [46,88,89]. The 275 nm band may be attributed to $n \rightarrow \pi^*$ or $\pi \rightarrow \pi^*$ transition corresponding to the partially deacetylated chitosan polymer [78,80,82,83].

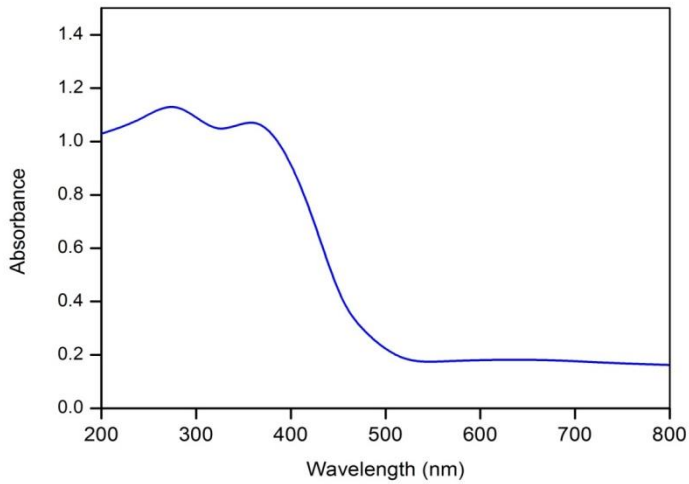

Fig. 4.7 UV-Vis spectrum of **PMoCh**.

4.2.2.7 ^{13}C NMR studies

The solid state ^{13}C NMR spectra of the pure polymer and the synthesized complex **PMoCh** shown in **Fig. 4.8(a)** and **4.8(b)**, respectively and data presented in **Table 4.4**, indicating modification of carbon signals as a result of anchoring of the Mo(VI) species to chitosan. The resonance positions were assigned on the basis of existing literature [90-92] although, the exact chemical shifts values may vary slightly depending on the crystallinity of the sample and the nature of technique employed *viz*., solid state or liquid state analysis. The spectrum of pure chitosan exhibited typical resonances due to C(1), C(2), C(4) and C(6) carbon atoms, respectively in addition to a resonance attributable to a combination of C(3) and C(5) carbon signals, as has been reported previously [90-92].

Table 4.4 Chemical shifts (ppm) of ^{13}C signals for chitosan (pure polymer) and for complex **PMoCh**

	C(1)	C(2)	C(3)/C(5)	C(4)	C(6)
Chitosan	106.3	58.7	76.8	85.1	62.3
PMoCh	100.7	57.1	75.2	93.5	61.1

For the complex **PMoCh**, the signal due to C(2) atom attached to the amine functions shifted to 57.1 ppm with a decrease in intensity, indicating the involvement of the amine group in complexation. The complexation through the hydroxyl group was also evident from the shifting of carbon signal to 75.2 ppm from its original value of 76.8 ppm observed in the spectrum of pure chitosan. In addition, C(1) and C(4) signals showed considerable shifts along with broadening indicating that the amino or hydroxyl containing sites are not the only atoms affected as a result of Mo complexion. It is notable that similar observations were made earlier by Guibal *et al*. during ^{13}C analysis of molybdate ion uptake by chitosan [90]. Apart from the above well-resolved resonances, very weak intensity signals were identified at around 174 and 23 ppm attributable to the -C=O and methyl (CH_3) group [**Fig. 4.8(a)**], respectively of the acetylated fraction of chitosan which remained unaltered in their position and pattern in the spectrum of the catalyst as well. Thus from the ^{13}C NMR spectral analysis it may be inferred that although the chitosan structure undergoes modification as a consequence of Mo(VI) ion co-ordination, the main backbone structure of the polymer remains unchanged during the process of metal ion complexation.

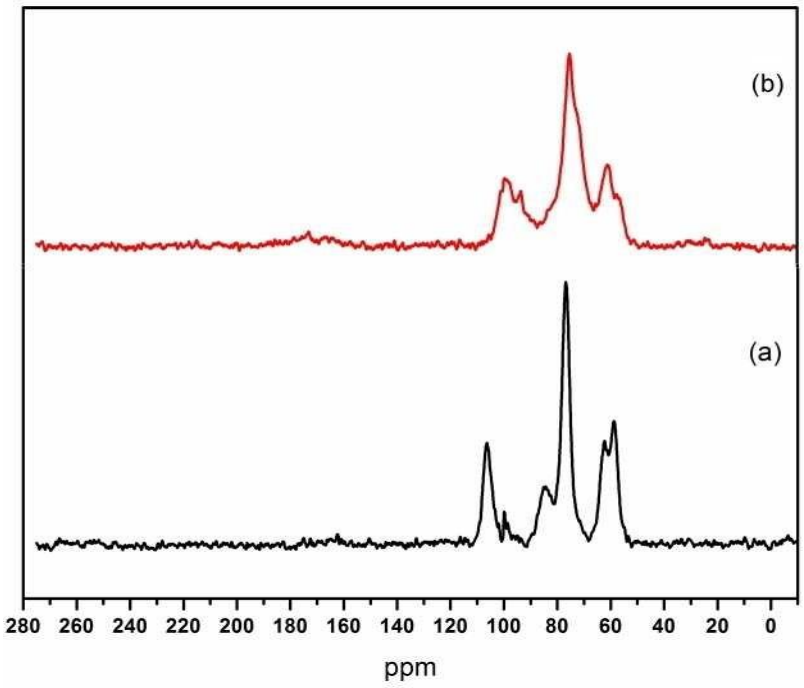

Fig. 4.8 Solid state ^{13}C NMR spectra of (a) chitosan and (b) **PMoCh**.

4.2.2.8 Thermal analysis

The TG-DTG plot of the complex **PMoCh** (**Fig. 4.9**) revealed that the compound (**PMoCh**) undergoes multiple step decomposition on heating to a temperature of 700 ^{0}C. After the initial degradation steps occurring in the temperature range of 50-97 ^{0}C due to the liberation of water molecules, the next degradation has been observed in the range of 140 to 153 ^{0}C with 6.6% weight loss. This step is attributable to the loss of peroxido groups of [$MoO_2(O_2)$] moieties anchored to the polymer. The subsequent step occurs between 169 ^{0}C to 310 ^{0}C, with a mass loss of 44.5% which has been ascribed to the cleavage of glycosidic linkage and degradation of the polymer. In case of pure chitosan, a single stage degradation takes place starting from 270 ^{0}C that continue up to 315 ^{0}C with a mass loss of 33.1% due to degradation of the polymer and deacetylation [68,71,78,93] after the initial dehydration step occurring below 100 ^{0}C (**Fig. 4.10**).

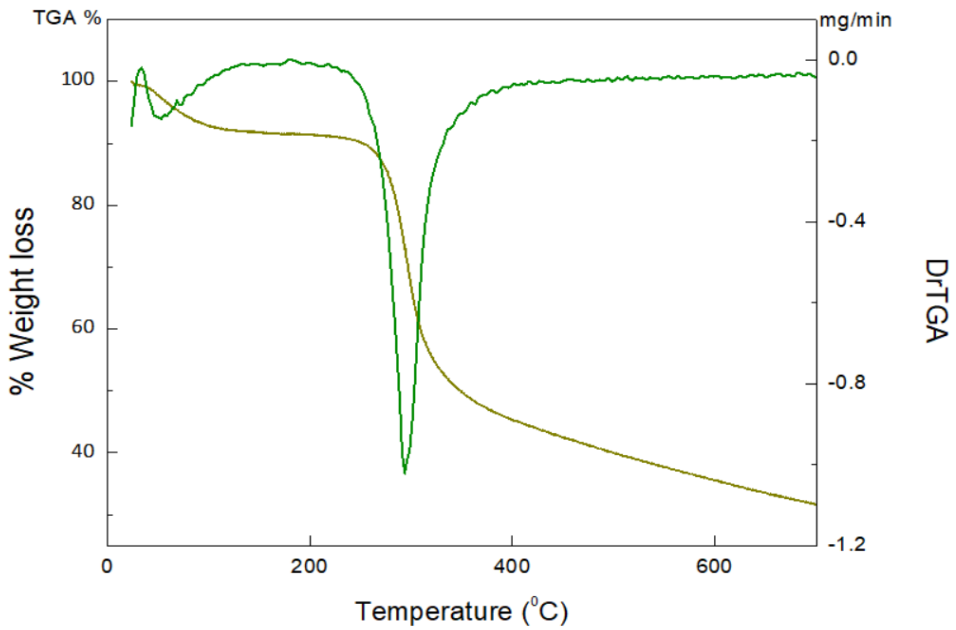

Fig. 4.9 TG-DTG plot of chitosan.

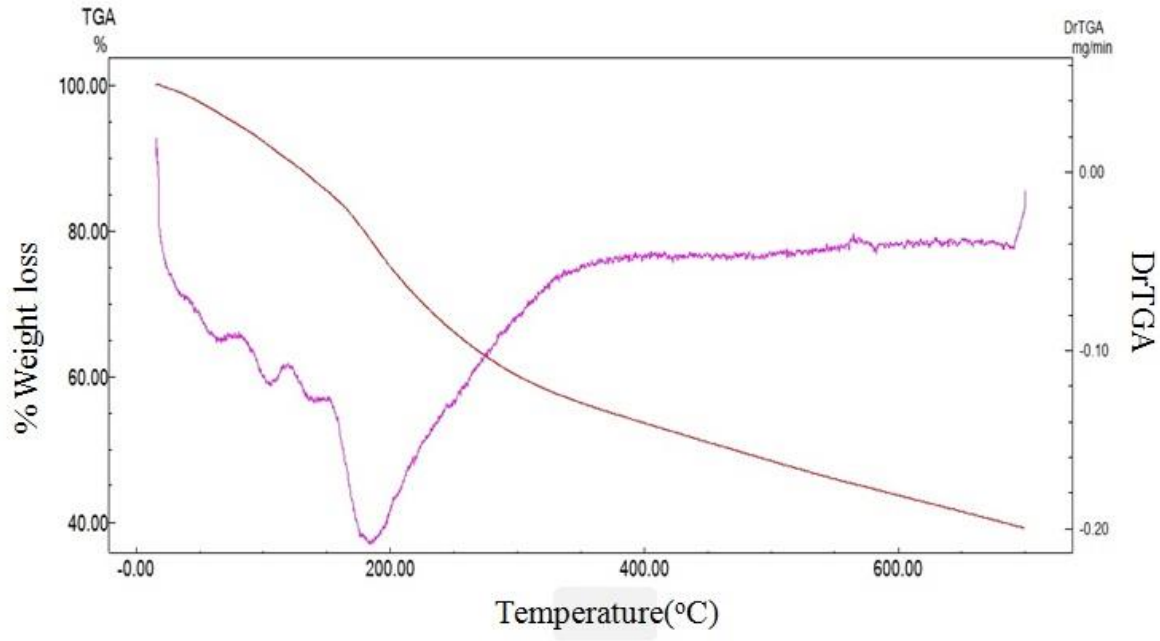

Fig. 4.10 TG-DTG thermogram of **PMoCh**.

Thus, decomposition step corresponding to the degradation of the chitosan support occurs at a relatively lower temperature range in the catalyst, **PMoCh** compared to free chitosan. The observations are in agreement with literature data which demonstrate that the complexation of chitosan usually leads to a lowering of its thermal stability [78,93]. The % residue remaining after complete degradation of the complex **PMoCh** was found to be 40.2 %, which was ascertained to be oxidomolybdenum species from the IR spectral analysis of the sample.

The structure proposed for the catalyst **PMoCh**, based on the above analysis, is represented schematically in **Fig. 4.11**. Different models have been proposed previously to describe the mode of metal ion-chitosan co-ordination such as “bridge model” and “pendant model” [76,79,88]. The structure of **PMoCh** shows simultaneous co-ordination of the Mo(VI) centre of the **pMo** moiety to the amino and OH group of chitosan to form a ‘pendant complex’.

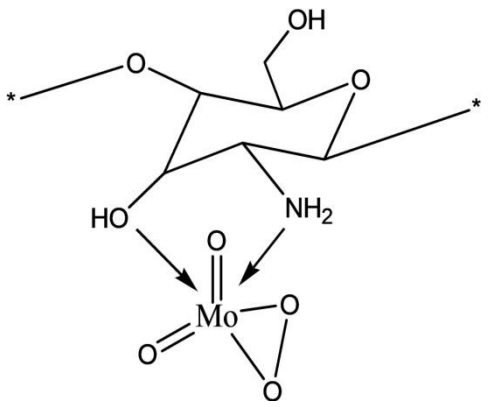

Fig. 4.11 Proposed structure of **PMoCh** (* represents polymer chain).

4.2.2.9 Density functional studies

We have carried out theoretical investigations in order to verify the feasibility of the structure proposed for the Mo-Chitosan (**PMoCh**) complex. The initial structure of the complex has been modelled on the basis of experimentally derived structural information (FTIR, Raman, TGA, EDX and elemental analysis). The optimized geometry of the molybdenum complex, representing a section of the polymer, is presented in **Fig. 4.12**. The structure shows one repeating unit of the polymer with one anchored Mo(VI) centre coordinated to two oxygen atoms of an η^2–peroxido group, doubly bonded to two oxygen atoms. The remaining two sites in the co-ordination sphere are occupied by one O atom and one N atom of the -OH and $-NH_2$ groups of chitosan, respectively in a trans configuration. The selected geometrical parameters of vibrational frequencies, bond length and bond angles shown in **Table 4.3** and **4.5**, are found to be in line with our experimental values. These experimental and theoretical values of complex **PMoCh** are in excellent agreement with the reported crystallographic data related to monoperoxido molybdenum complexes with coordination environment containing N, O- or O- donor co-ligands [94,95].

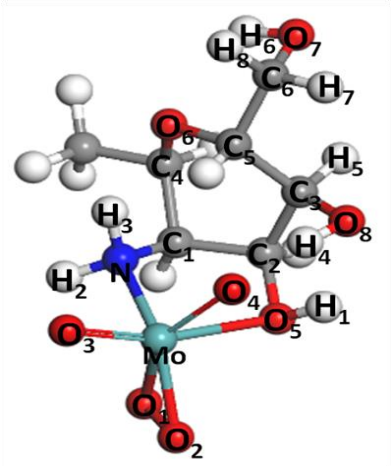

Fig. 4.12 Optimized geometry for complex **PMoCh**. Colors: light blue is molybdenum, red is oxygen, grey is carbon and white balls represent hydrogen atoms.

Table 4.5 Selected bond lengths (Å) and bond angles (degree) for **PMoCh** calculated using density functional theory (DFT) as implemented in DMol[3] package

Structural index[a]	Calculated values	Structural parameter	Calculated values
Mo-O1	1.991	O6-C4	1.426
Mo-O2	1.899	O6-C5	1.438
Mo-O3	1.713	O5-C2	1.398
Mo-O4	1.769	O7-H6	0.979
Mo-O5	2.495	O8-H4	1.024
Mo-N	2.149	C3-O8	1.399
N-C1	1.468	C1-C4	1.512
N-H2	1.038	C1-C2	1.501
N-H3	1.026	C3-C5	1.537
N-H1	1.002	∠O1-Mo-O2	43.18
C3-H5	1.102	∠O3-Mo-O4	106.08
C6-H7	1.099	∠Mo-O1-O2	72.19
C6-H8	1.104	∠H2-N-H3	107.44

[a]See Fig. 4.12 for the atomic numbering.

4.2.3 Catalytic activity of the supported complex, PMoCh (4.1)

4.2.3.1 Oxidation of sulfides to sulfoxides- Optimization of reaction condition

Selective oxidation of various organic sulfides with 30% H_2O_2 could be achieved in neat water in presence of catalytic amounts of compound **PMoCh**. Initially, we have conducted an exploratory experiment using methyl phenyl sulfide as a model substrate maintaining molar ratio of substrate:oxidant at 1:2 and catalyst (Mo):substrate ratio at 1:1000 in water, at ambient temperature under magnetic stirring. Under these conditions the reaction was observed to proceed smoothly to afford sulfoxide as the sole product with 100% conversion and reasonably good TOF and TON values. Subsequently, we have optimized the reaction conditions for selective sulfoxidation by screening the effect of key parameters such as substrate:oxidant stoichiometry, catalyst amount, solvent type and reaction temperature. The details of the observations are depicted in **Table 4.6**.

Effect of H_2O_2 concentration

In order to assess the effect of H_2O_2 concentration on the selective sulfoxidation reaction, we have examined three different equivalents of H_2O_2 with respect to MPS under otherwise identical reaction condition. As shown in **Table 4.6** (entries 1, 2 and 3) with an increase in the amount of oxidant the rate of the reaction was found to increase monotonously affording a TOF of 1140 h^{-1} with 4 equivalents of H_2O_2. It is notable that even with 4 equivalents of oxidant, the reaction retained its sulfoxide selectivity without any over oxidation of sulfoxide to sulfone.

Effect of catalyst amount

The amount of catalyst used was observed to affect the rate of the sulfide oxidation substantially. As revealed by the data presented in **Table 4.6**, an increase in catalyst amount speeded up the MPS oxidation considerably without affecting the selectivity, although the reaction resulted in a drastic fall in the TOF value. On the other hand, reducing the catalyst amount led to a consistent improvement in TOF of the process (**Table 4.6**, entries 3, 4 and 5). Thus, to obtain best TOF in aqueous medium without compromising the selectivity, a catalyst (Mo):substrate molar ratio of 1:2000 with substrate:oxidant ratio maintained at 1:4 was found to be optimal. That the catalyst played

Table 4.6 Optimization of reaction conditions for **PMoCh** catalyzed selective oxidation of methyl phenyl sulfide (MPS) by 30% H_2O_2[a]

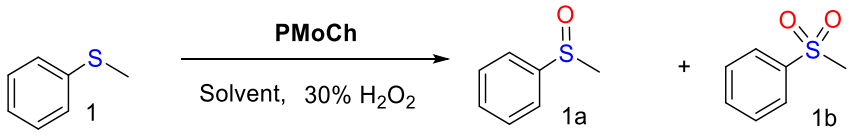

Entry	Molar ratio (Mo:MPS)	Sub:H_2O_2	Solvent	Time (min)	Isolated yield (%)	1a:1b	TON[b]	TOF[c] (h^{-1})
1	1:1000	1:2	H_2O	100	91	100:0	910	546
2	1:1000	1:3	H_2O	75	90	100:0	900	720
3	1:1000	1:4	H_2O	50	95	100:0	950	1140
4	1:500	1:4	H_2O	30	90	100:0	450	900
5	**1:2000**	**1:4**	**H_2O**	**65**	**97**	**100:0**	**1940**	**1790**
6[d]	**1:2000**	**1:4**	**H_2O**	**65**	**48**	**74:26**	**960**	**886**
7[e]	--	1:4	H_2O	65	15	100:0	--	--
8	1:1000	1:1	MeOH	80	90	100:0	900	675
9	1:1000	1:2	MeOH	20	93	100:0	930	2790
10	1:500	1:2	MeOH	10	91	100:0	455	2730
11	1:1500	1:2	MeOH	32	90	100:0	1350	2556
12	1:2000	1:2	MeOH	40	94	100:0	1880	2850
13	1:2000	1:3	MeOH	30	94	100:0	1880	3760
14	**1:2000**	**1:4**	**MeOH**	**20**	**98**	**100:0**	**1960**	**5880**
15[d]	**1:2000**	**1:4**	**MeOH**	**20**	**44**	**58:42**	**880**	**2640**
16[e]	--	1:4	MeOH	20	18	100:0	--	--
17	1:2000	1:4	EtOH	20	88	100:0	1760	5280
18	1:2000	1:4	CH_3CN	25	90	100:0	1800	4320

[a]All the reactions were carried out with 5 mmol of substrate in 5 mL of solvent. Catalyst amount = 1.4 mg for 0.0025 mmol of Mo. [b]TON (turnover number) = mmol of product per mmol of catalyst. [c]TOF (turnover frequency) = mmol of product per mmol of catalyst per hour. [d]Using Na_2MoO_4 as catalyst (0.51 mg, 0.0025 mmol of Mo). [e]Blank experiment without any catalyst.

a crucial role in facilitating the formation of the desired product was also evident from the result of a control experiment performed without the catalyst under optimized condition. In absence of the catalyst a poor conversion of ≤ 15% was obtained within the stipulated reaction time. Moreover, in order to compare the performance of the heterogeneous phase reaction with the homogeneous one, the oxidation reaction was conducted under optimized condition by adding soluble Na_2MoO_4 (Mo: MPS = 1:2000) in lieu of the catalyst. The results revealed that **(Table 4.6**, entries 6 and 15) although *in situ* generated soluble **pMo** species also catalyzed the MPS oxidation, the reaction remained incomplete and non-selective leading to the formation of sulfoxide and sulfone in the ratio of 74:26. That the immobilization of **pMo** species on chitosan support resulted in remarkable improvement of catalytic efficiency of **pMo** derivative, both in terms of activity and selectivity, has been confirmed from these observations.

Effect of solvent nature

Since solvents have been known to have immense influence on the activity and selectivity of catalysts in sulfoxidation reaction, we considered it imperative to examine the activity of the catalyst in some common organic solvents, other than water. The solvent effect was assessed using environmentally safer organic solvents such as methanol, ethanol and acetonitrile in the oxidation of MPS. As mentioned in Chapter 3, use of toxic chlorinated solvents was strategically avoided in the present study as well. The results presented in **Table 4.6** demonstrate that the catalytic protocol for sulfoxidation is compatible with each of the tested organic solvents. In fact, the catalyst turned out to be nearly 3-fold more potent in organic solvents (**Table 4.6**, entries 14, 17 and 18) compared to aqueous medium. Methanol emerged as the best solvent in terms of selectivity-activity profile of the reaction providing good TOF even with 1 equivalent of H_2O_2 (**Table 4.6**, entry 8). The superior activities observed in organic solvent are likely to be due to the high solubility of MPS in these solvents. It is thus remarkable that the same heterogeneous catalyst **PMoCh** enabled us to attain selective sulfoxidation in neat water as well as in organic solvent, under mild reaction condition testifying to the versatility of the catalyst.

Subsequent to optimization of the right conditions for sulfoxidation as shown in **Scheme 4.1**, a series of structurally diverse organic sulfides were subjected to the oxidation reaction using **PMoCh-**H_2O_2 system in experiment performed independently

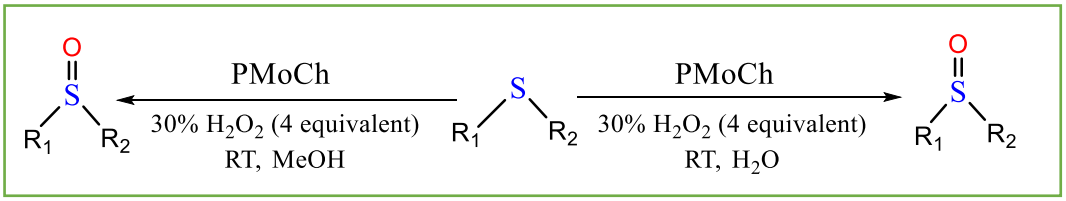

Scheme 4.1 Optimized reaction conditions for the selective oxidation of sulfides to sulfoxides by catalyst **PMoCh**.

using water or methanol as solvent. The results illustrated in **Tables 4.7** and **4.8** show that variously substituted aliphatic as well as aromatic substrates were selectively and completely transformed in presence of the catalyst **PMoCh** into corresponding sulfoxides with excellent TOF and TON values. Significantly, no over oxidation of sulfoxide to sulfone was observed in any of the tested substrates under the investigated condition even on prolonging the reaction time. It is also noteworthy that irrespective of the nature of solvent used, oxidation of dimethyl sulfide was observed to proceed at the fastest rate (Entry 2, **Table 4.7** and **4.8**) providing a TOF of 3760 h^{-1} in water (TOF as high as 11,280 h^{-1} in MeOH), whereas in case of diphenyl sulfide the reaction was the slowest (Entry 9, **Table 4.7** and **4.8**). In general, aliphatic sulfides were found to be oxidized at a faster rate compared to allylic and vinylic sulfides, which is not unusual. As sulfide oxidation by H_2O_2 has been known to occur *via* an electrophilic addition reaction of oxygen atom to the substrate, it is expected that sulfides with higher electron density on sulfur atoms would react faster compared to aromatic as well as other conjugated systems *viz*., vinylic and allylic sulfides [96,97]. Thus, the observed trend in variation of rates of reaction across the substrates used is in accord with the decreasing nucleophilicity of the thioethers examined. An additional salient feature of the methodology is the excellent chemoselectivity of the catalyst towards sulfur group of substituted sulfides with co-existing oxidation prone functional groups. Thus, alcoholic sulfoxides were obtained without affecting any other functional group transformation (**Table 4.7**, entry 8 and **Table 4.8** entry 8), whereas allylic sulfides were chemoselectively oxidized without epoxidation of C=C (**Table 4.7**, entry 7 and **Table 4.8**, entry 7).

Table 4.7 Selective oxidation of sulfides to sulfoxides with 30% H_2O_2 catalyzed by **PMoCh** in H_2O[a]

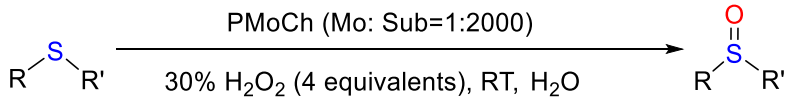

Entry	Substrate	Mo:MPS	MPS: H_2O_2	Time(min)	Isolated yield (%)	Sulfoxide: Sulfone	TON[b]	TOF[c] (h^{-1})
1	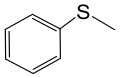	1: 2000	1:4	65	97	100:0	1940	1790
				65	94[d]	100:0	1880	1735
				65	96[e]	100:0	1920	1772
2	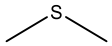	1: 2000	1:4	30	94	100:0	1880	3760
3	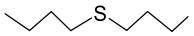	1: 2000	1:4	60	96	100:0	1920	1920
4	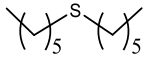	1: 2000	1:4	65	93	100:0	1860	1716
5	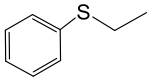	1: 2000	1:4	80	96	100:0	1920	1440
6	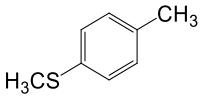	1: 2000	1:4	60	97	100:0	1940	1940

Continued..

7	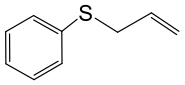	1: 2000	1:4	135	96	100:0	1920	853
8	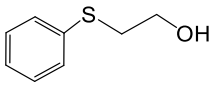	1: 2000	1:4	110	94	100:0	1880	1025
9	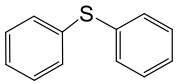	1:2000	1:4	360	92	100:0	1840	306

[a]Reactions carried out with 5 mmol substrate, 20 mmol 30% $H_2O_2$and catalyst (1.4 mg, 0.0025 mmol of Mo) in 5 mL H_2O at RT.
[b]TON (turnover number)= mmol of product per mmol of catalyst.
[c]TOF(turnover frequency) = mmol of product per mmol of catalyst per hour.
[d]Yield of 6th reaction cycle.
[e]Scale up data (7.5 g of MPS).

Table 4.8 Selective oxidation of sulfides to sulfoxides with 30% H_2O_2 catalyzed by **PMoCh** in MeOH[a]

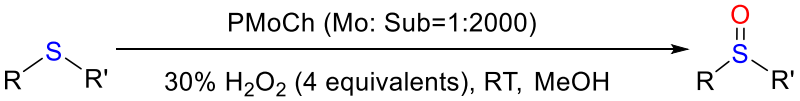

Entry	Substrate	Mo:MPS	MPS: H_2O_2	Time (min)	Isolated yield (%)	Sulfoxide: Sulfone	TON[b]	TOF[c] (h^{-1})
1	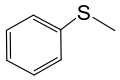	1:2000	1:4	20	98	100:0	1960	5880
		1:2000	1:4	20	94[d]	100:0	1880	5640
		1:2000	1:4	20	96[e]	100:0	1920	5760
2	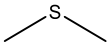	1:2000	1:4	10	94	100:0	1800	11280
3	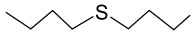	1:2000	1:4	15	96	100:0	1920	7680
4	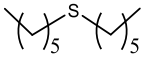	1:2000	1:4	20	95	100:0	1900	5700
5	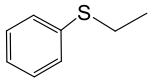	1:2000	1:4	25	94	100:0	1880	4512
6	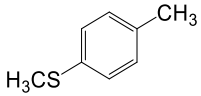	1:2000	1:4	20	97	100:0	1940	5820

Continued...

7	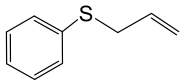	1:2000	1:4	35	94	100:0	1880	3222
8	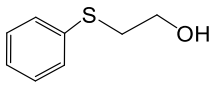	1:2000	1:4	45	96	100:0	1920	2560
9	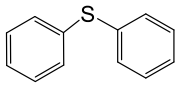	1:2000	1:4	180	94	100:0	1880	626

[a]Reactions carried out with 5 mmol substrate, 20 mmol 30% H_2O_2 and catalyst (1.4 mg, 0.0025 mmol of Mo) in 5 mL methanol at RT.

[b]TON(turnover number)= mmol of product per mmol of catalyst.
[c]TOF(turnover frequency) = mmol of product per mmol of catalyst per hour.
[d]Yield of 6th reaction cycle.
[e]Scale up data (7.5 g of MPS).

It is pertinent to mention that in view of the environmentally benign aspect, we have chosen room temperature for our studies. Moreover, oxidations were performed at natural pH attained by the reaction mixture, as we focused on accomplishing the desired transformations under mild condition precluding the use of acid or other hazardous auxiliaries. Although previous reports [98,99], demonstrated that catalytic activity of peroxidometallates can be significantly improved in presence of acidic additives [47,100,101], no attempt has been made to adjust the pH of the reaction in the present study.

4.2.3.2 Utilization efficiency of H_2O_2

The utilization efficiency of H_2O_2 (defined as: 100 × mol of H_2O_2 consumed in the formation of the oxidized product/mol of H_2O_2 converted) was observed to be consistently higher than 90% in the oxidations conducted in methanol [57]. On the other hand, H_2O_2 efficiency or effective use of H_2O_2 was noted to be relatively less (85–90%) for similar reactions carried out using water as solvent. This may be due to the relatively longer time required for completion of the water-based reactions, which is likely to facilitate direct decomposition of H_2O_2 [37,41,46,47].

The potential of the developed methodology for relatively larger scale synthetic application has been ascertained in both aqueous as well as organic medium by performing the oxidation of MPS at ten-fold scale under optimized condition as shown in **Table 4.7**, entry 1^e and **Table 4.8**, entry1^e.

4.2.3.3 Recyclability of the catalyst

For the practical usefulness of a catalytic protocol, the stability and recyclability of the catalyst are of vital importance. Due to its heterogeneous nature, the newly synthesized catalyst **PMoCh** enabled easy separation from the spent reaction mixture by filtration which could be reused without further conditioning. The recyclability of the catalyst in subsequent cycles of reaction was examined under optimized reaction condition by charging the spent catalyst with H_2O_2, a fresh lot of MPS and the respective solvent (water or methanol). To our satisfaction, it was found that the catalyst remained active even after being reused for six cycles in water as well as in methanol (**Fig. 4.13**) without any loss in selectivity.

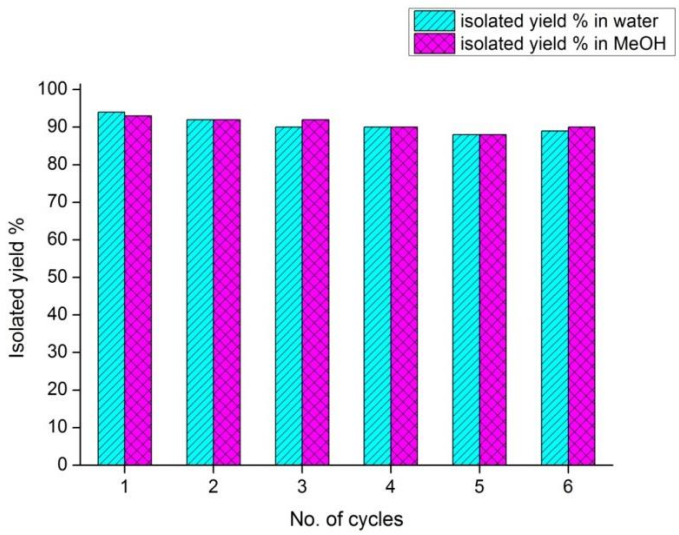

Fig. 4.13 Recyclability of **PMoCh** for the selective oxidation of MPS to sulfoxide in H_2O and MeOH.

The highest overall TOF of *ca*. 10,580 h^{-1} was obtained after 6 catalytic cycles in water (*ca*. 34,920 h^{-1} in MeOH). Although a direct comparison of our findings with those reported in the literature is difficult to be drawn due to variable reaction conditions and absence of TOF and TON values in many of these studies, our results appear to demonstrate superior activity of the catalyst **PMoCh** over most of the other homogeneous or heterogeneously catalyzed sulfoxidation conducted in water [40-43].

In order to further ascertain the stability of the catalyst during the cycles of oxidation the recovered catalyst was characterized by FTIR, ICP-OES and EDX spectral analysis. The FTIR spectrum of the used catalyst was observed to be identical with corresponding spectrum of the original catalyst showing the signature absorptions corresponding to chitosan and metal peroxido moiety (**Fig. 4.14**).

Furthermore, no significant quantitative loss in Mo content was indicated by ICP and EDX analysis data compared to the fresh catalyst. Thus, it has been confirmed that the structural integrity of the catalyst remained intact even after repeated cycles of oxidation.

4.2.3.4 Test for heterogeneity of the reaction

Separate experiments were performed using MPS as the substrate under optimized condition, in order to confirm the heterogeneity of the oxidation and to examine whether there is any leaching of the active **pMo** species from the chitosan supported catalyst into

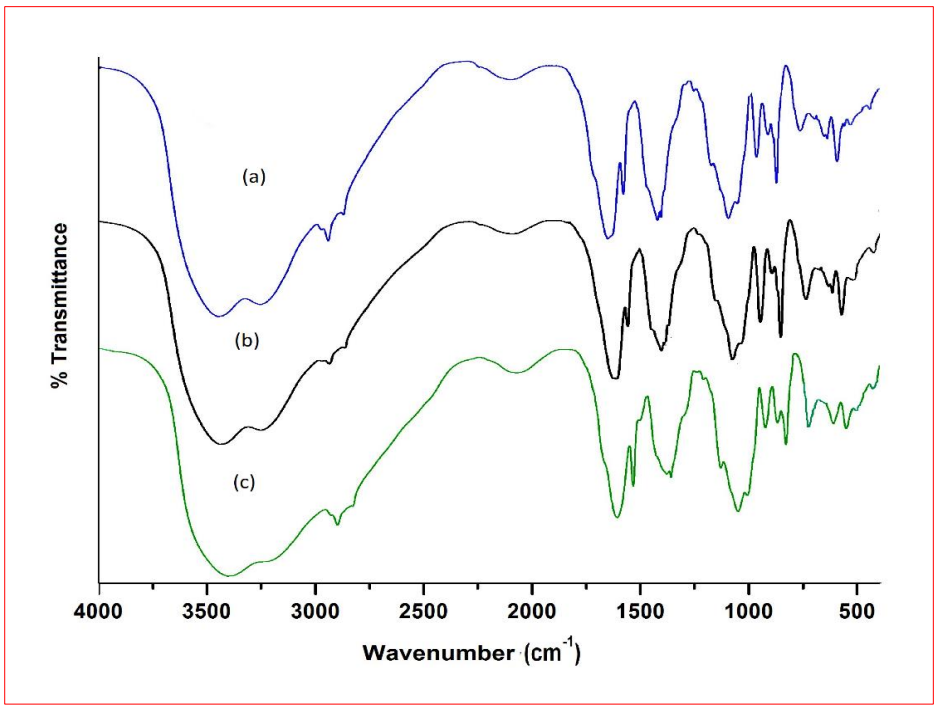

Fig. 4.14 IR spectra of (a) original catalyst **PMoCh**, (b) catalyst **PMoCh** regenerated after 6th cycle in water and (c) catalyst **PMoCh** regenerated after 6th cycle in MeOH.

the reaction solution. Subsequent to completion of the reaction the solid catalyst was separated by filtration and the filtrate collected was transferred to a reaction vessel.

After addition of a fresh lot of MPS and H_2O_2 to the filtrate, the reaction was allowed to continue for another 1 h under optimized condition. After removal of the catalyst, the reaction was noted to remain incomplete under these condition providing, ≤ 16% conversion in MeOH (14% in water). These values are close to the yield obtained in case of blank experiment conducted in absence of the catalyst (**Table 4.6**, entries 7 and 16). Moreover, the absence of molybdenum in the filtrate after isolating the solid catalyst was confirmed by ICP analysis, thereby negating the possibility of catalyst leaching. These data unambiguously suggest the heterogeneous nature of the catalytic process.

4.2.3.5 The proposed catalytic cycle

A credible scheme of reactions for selective oxidation of sulfides to the corresponding sulfoxide outlined in **Fig. 4.15**, is proposed which satisfactorily explains our experimental findings. The mechanism of action of peroxidomolybdenum complexes

in organic oxidations have been extensively investigated over the past decades [46,102-107]. It has been established that a **pMo** species to be catalytically active in oxygen transfer reactions of organic substrates, formation of a oxidodiperoxido Mo(VI) configuration is a pre-requisite [46,108,102,103].

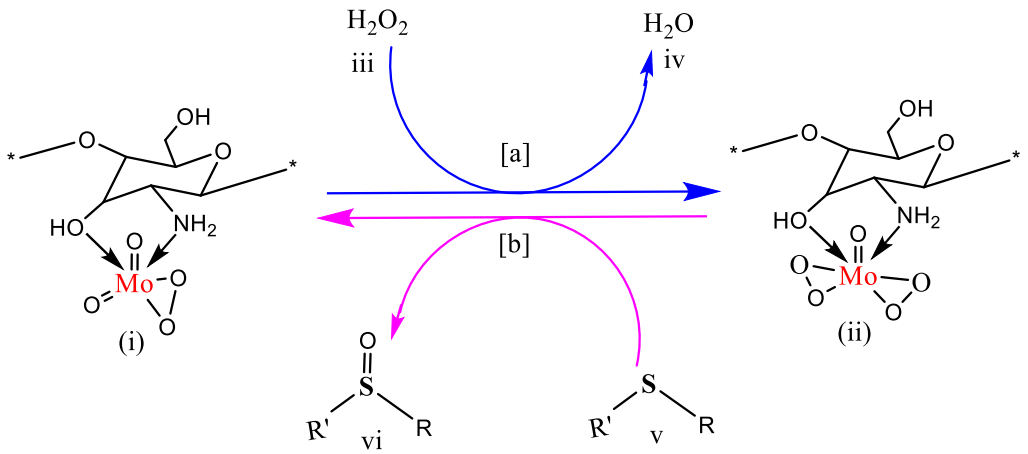

Fig. 4.15 Proposed catalytic cycle.

In the present study therefore, it is reasonable to expect that in the first step, the monoperoxidomolybdate species **I** would react with H_2O_2 to generate an active diperoxidomolybdate species **II** (reaction a). Since the electrophilicity of the peroxidomolybdate species is known to be much higher than that of H_2O_2 [56], in the subsequent step (reaction b), facile transfer of electrophilic oxygen from species **II** to the substrate **V** is likely to occur to yield the corresponding sulfoxide **VI**. The sulfoxidation reaction is accompanied by concomitant regeneration of the original monoperoxidomolybdate catalyst **I**, which also completes the catalytic cycle (reaction b).

4.3 Section B:

Water soluble polymer supported peroxidomolybdenum complexes catalyzed selective sulfoxidation in water: a sustainable approach

4.3.1 Experimental section

4.3.1.1 Synthesis of water soluble peroxidomolybdenum complexes,

[$MoO(O_2)_2$(sulfonate)]–PS [PS = poly(sodium vinyl sulfonate)] (PSMo) (4.2) and [$Mo_2O_2(O_2)_4$(carboxylate)]–PA [PA = poly(sodium acrylate)] (PAMo) (4.3)

The catalysts **PAMo** and **PSMo** were obtained according to the method reported earlier by our group [58,59].

To a solution of molybdic acid (0.64 g, 4.0 mmol for compounds **PAMo** or 1.84 g, 11.50 mmol for **PSMo**) dissolved in 30% H_2O_2 (12 mL, 105.84 mmol for **PAMo** or 15 mL, 132.30 mmol for **PSMo**) maintaining the temperature at 30-40 ^{0}C, 1.5 g of respective polymer was added with constant stirring. The resulting mixture was stirred for an hour in an ice bath. The pH of the reaction solution at this stage was recorded to be *ca.* 2, which was adjusted at 5 by dropwise addition of 8 M NaOH solution. On addition of about 50 mL of pre-cooled acetone to the reaction solution with constant stirring, a red colored pasty product separated out which on repeated treatment with acetone turned into a microcrystalline solid. The compound was separated by centrifugation, washed 3-4 times with cold acetone and dried *in vacuo* over concentrated sulfuric acid. The compound was subsequently dried by heating up to 70 ^{0}C under nitrogen atmosphere.

4.3.1.2 General procedure for catalytic oxidation of sulfides to sulfoxides

In a typical reaction, organic substrate (5 mmol) was added to a solution of catalyst [**PAMo** (3.4 mg) or **PSMo** (4.9 mg), containing 0.005 mmol of Mo] and 30% H_2O_2 (2.26 mL, 20 mmol) in 5 mL of water. The molar ratio of substrate:H_2O_2 and that of catalyst (Mo): substrate was maintained at 1:4 and 1:1000, respectively. The reaction was conducted at room temperature under magnetic stirring. The reaction progress was monitored by thin layer chromatography (TLC) and GC. After completion, the product and unreacted organic substrates were extracted with diethyl ether, dried over anhydrous sodium sulfate and distilled under reduced pressure to remove excess solvent. The crude product obtained was purified by column chromatography on silica gel with ethyl acetate-hexane (1:9 v/v) as the eluent. The product obtained was characterized by a combination of IR, ^{1}H NMR, ^{13}C NMR spectroscopy and melting point determination (for solid products) (**Appendix I**).

4.3.1.3 Procedure for regeneration of the catalyst

The recyclability of each of the catalysts was examined by using MPS as the substrate adopting the following procedures. For selective sulfoxidation, the catalyst could be regenerated and recycled *in situ*. After completion of the reaction run, the aqueous part of the reaction mixture was treated with 30% H_2O_2 (2.26 mL, 20 mmol) followed by a fresh batch of substrate and the reaction was conducted under optimized condition in the same manner as reported in the first run (Above section). The progress of the reaction was monitored by thin layer chromatography (TLC) and GC. The process has been repeated for ten cycles of reaction.

In an alternative procedure, the recovered catalyst could also be isolated as solid and reused in subsequent cycles of oxidation. The aqueous part of the spent reaction mixture was transferred to a beaker and treated with 30% H_2O_2 (2.26 mL) in order to replenish the peroxido content of the catalyst state. To this solution pre-cooled acetone was added with constant stirring until the solid catalyst separated out which was isolated following the same work up procedure mentioned under Section 4.3.1.1. The dried solid catalyst was used in subsequent reaction cycle conducted under optimized condition.

4.3.2 Results and discussion

4.3.2.1 Oxidation of sulfides to sulfoxides

The macro complexes **PSMo** and **PAMo** of the type shown in **Fig 4.16 (a)** and **4.16 (b)** respectively, were examined for their catalytic efficiency in selective sulfoxidation reaction with 30% H_2O_2 as terminal oxidant under aqueous conditions. Optimization studies were carried out employing thioanisole as the representative substrate and **PSMo** as the catalyst, at ambient temperature. The details of the study are summarized in **Table 4.9**. Based on the assessment of the effect of various reaction parameters as illustrated in **Table 4.9**, for achieving best results in aqueous medium without compromising the selectivity, we have decided to maintain a Mo: substrate molar ratio of 1:1000 and substrate:H_2O_2 at 1:4 for subsequent reactions (**Table 4.9**, entry 7). It is noteworthy that the procedure worked well even at Mo: substrate ratio of 1:2000 with 2 equivalents of H_2O_2 affording a good TOF, *albeit* the reaction time increased considerably. On the other hand, increase in the amount of the oxidant led to a significant enhancement of the rate of the reaction, enabling us to achieve over eight fold improvement of TOF

(**Table 4.9**, entry 7) simply by using 4 equivalents of H_2O_2, without altering other reaction parameters. Incidentally, the reaction condition optimized with the **pMo** catalysts was found to be similar to the one established for the water soluble **pTi** catalysts **3.1-3.3** (Chapter 3, **Table 3.8**). Thus, under identical reaction condition, **pMo** catalysts are found to be more efficient with a TOF value of 5880 h^{-1} compared to TOF obtained for their Ti containing analogues (3880 h^{-1}).

Result of a blank experiment conducted in absence of the catalyst under otherwise analogous reaction conditions (**Table 4.9**, entry 15), clearly showed the indispensability of the catalyst in obtaining the targeted product at a remarkably faster rate. Furthermore, the distinctly superior activity displayed by the supported homogeneous catalyst relative to the neat **pMo** species (**Table 4.9**, entry 14) made it apparent that immobilization of **pMo** species on the WSP support indeed led to an enhancement of the catalytic efficiency **pMo** derivatives both in terms of yield, as well as product selectivity. We have also performed the oxidation reactions under identical condition using the free polymer PA or PS in lieu of the **pMo** supported catalysts. The yield obtained in each case was nearly the same as that obtained from the blank experiment conducted in absence of the catalyst (**Table 4.9**, entry 16). The results clearly demonstrated that the chosen pristine polymers have no observable effect on the course of the oxidation reaction.

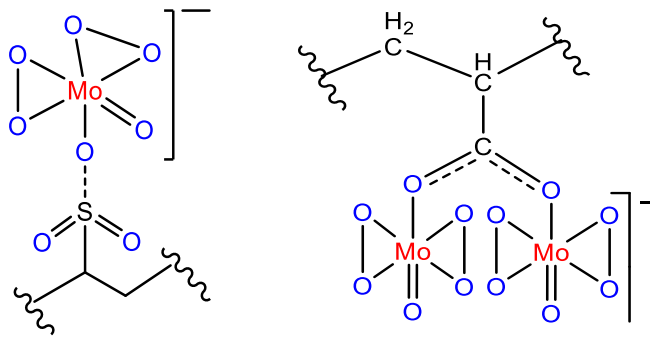

(a) (b)

Fig. 4.16 Peroxido compounds of Mo(VI) under investigation in the current study. Structures of (a) **PSMo** and (b) **PAMo** [58,59]. "∿∿" represents polymer chain.

Table 4.9 Optimization of reaction conditions for **PSMo** catalyzed selective oxidation of methyl phenyl sulfide (MPS) to sulfoxide by 30% H_2O_2[a]

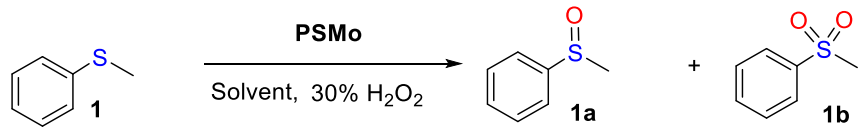

Entry	Molar ratio (Mo:MPS)	H_2O_2 (equiv.)	Solvent	Temp.	Time (min)	Isolated yield (%)	**1a:1b**	TON[b]	TOF[c] (h^{-1})
1	1:1000	1	H_2O	RT	80	91	100:00	910	682
2	1:1000	2	H_2O	RT	60	96	100:00	960	960
3	1:500	2	H_2O	RT	45	94	100:00	470	627
4	1:1500	2	H_2O	RT	85	97	100:00	1455	1027
5	1:2000	2	H_2O	RT	100	98	100:00	1960	1176
6	1:1000	3	H_2O	RT	25	97	100:00	970	2328
7	**1:1000**	**4**	**H_2O**	**RT**	**10**	**98**	**100:00**	**980**	**5880**
8	1:1000	2	MeOH	RT	80	97	100:00	970	727
9	1:1000	2	EtOH	RT	65	97	100:00	970	895
10	1:1000	2	CH_3CN	RT	100	98	61:39	980	588
11	1:1000	2	$CHCl_3$	RT	80	8	87:13	80	60
12	1:1000	2	CH_2Cl_2	RT	80	13	84:16	130	98
13	1:1000	2	H_2O	60°C	20	90	100:00	900	2700
14[d]	1:1000	4	H_2O	RT	10	16	68:32	160	960
15[e]	_	4	H_2O	RT	10	13	100:00	_	_
16[f]	_	4	H_2O	RT	10	14	100:00	_	_

[a]All the reactions were carried out with 5 mmol of substrate in 5 mL of solvent. Catalyst amount = 4.90 mg for 0.005 mmol of Mo. [b]TON (turnover number) = mmol of product per mmol of catalyst. [c]TOF (turnover frequency) = mmol of product per mmol of catalyst per hour. [d]Using Na_2MoO_4 as catalyst (1.03 mg, 0.005 mmol of Mo). [e]Blank experiment without any catalyst. [f]Reaction in presence of free poly (sodium vinyl sulfonate) (4.42 mg).

A survey of the solvent effect on sulfoxidation, showed water to be the best solvent as indicated by both product selectivity as well as superior TOF. Interestingly, the methodology for sulfoxidation has been found to be compatible in presence of other polar protic organic solvents such as methanol and ethanol (**Table 4.9**, entries 8 and 9), although not very effective in non-polar solvents (**Table 4.9**, entries 11 and 12). In fact, the compatibility of the catalytic procedure in a variety of solvents emerged as a remarkable and common feature shared by the homogeneous **pMo** catalysts with their heterogeneous counterpart **PMoCh,** as well as their WSP bound **pTi** containing analogue, **3.1**-**3.3**. It is also notable that both the catalysts, dissolve completely in the water miscible solvents *viz.*, methanol, ethanol and acetonitrile, in presence of aqueous H_2O_2 and thus provided homogeneity of the catalytic process.

It is worthy to note that in the present work all transformations occurred at the natural pH of the reaction medium. Also, we have chosen room temperature for our studies although, a significant increase in TOF could be attained at a moderately higher temperature as shown in **Table 4.9** (entry 13).

Having established the optimized reaction conditions for selective sulfoxidation of the model substrate, we extended the study to a range of structurally diverse sulfides such as dialkyl, diaryl, aryl alkyl, aryl vinyl, aryl alcohol as well as dibenzothiophene (DBT).The results depicted in **Table 4.10** reveal that excellent yield with complete selectivity could be obtained in presence of each of the catalysts **PSMo** and **PAMo**, across the series of substrates examined, affording the corresponding sulfoxide as the sole product. Significantly, no over oxidation of sulfoxide to sulfone was noted under the investigated conditions.

The catalyst **PSMo**, supported on poly (sodium vinyl sulfonate) with monomeric oxidodiperoxidomolybdenum moieties was observed to display consistently superior activity compared to the catalyst **PAMo** having dimeric **pMo** units. The distinct influence of the co-ordination sphere on catalytic activity of these supported **pMo** catalysts is thus apparent from the data.

The methodology worked well for both aliphatic as well as aromatic substrates, *albeit* the rates of oxidation showed variations depending on the nature of the substrate and substituents attached. It was therefore not surprising that the protocol enabled us to attain the highest TOF value of 11,520 h^{-1} (for **PSMo**) for dimethyl sulfide oxidation

Table 4.10 Selective oxidation of sulfides to sulfoxides with 30% H_2O_2 catalyzed by **PSMo** and **PAMo**[a]

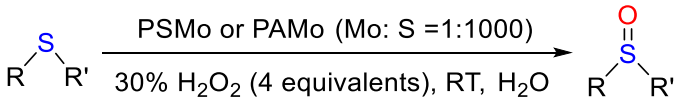

Entry	Substrate	PSMo				PAMo			
		Time (min)	Isolated yield (%)	TON[b]	TOF[c] (h^{-1})	Time (min)	Isolated yield (%)	TON[b]	TOF[c] (h^{-1})
1	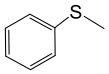	10	98	980	5880	15	98	980	3920
		10	96[d]	960	5760	15	95[d]	950	3800
		10	97[e]	970	5820	15	96[e]	960	3840
2	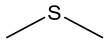	5	96	960	11520	10	93	930	5580
3	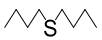	8	97	970	7275	12	96	960	4800
4	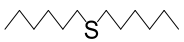	8	96	960	7200	12	95	950	4750
5	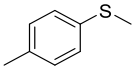	10	94	940	5640	15	97	970	3880
6	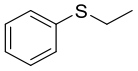	15	98	980	3920	25	96	960	2307
7	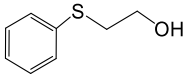	50	97	970	1164	70	93	930	797

Continue…

8	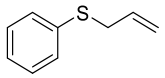	40	95	950	1425	60	93	930	930
9	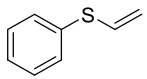	130	97	970	448	155	96	960	372
10	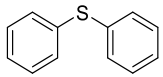	150	96	960	384	180	94	940	313
11[f]	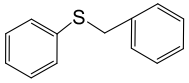	150	98	980	392	160	97	970	363
12[g]	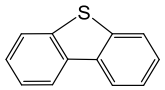	11h	90	90	8.1	11h	89	89	8.0

[a]All reactions were carried out in 5 mmol substrates, 20 mmol 30% H_2O_2 and catalyst (0.005 mmol of Mo) in 5 mL H_2O at RT, unless otherwise indicated. [b]TON (turnover number) = mmol of product per mmol of catalyst. [c]TOF (turnover frequency) = mmol of product per mmol of catalyst per hour. [d]Yield of 10th reaction cycle. [e]Scale up data (7.5g of MPS). [f]Reaction condition: 5 mmol substrate, 20 mmol 30% H_2O_2 and catalyst (0.005 mmol of Mo) in 5mL methanol at RT. [g]Reaction condition: 5 mmol substrate, 20 mmol 30% H_2O_2 and catalyst (0.05 mmol of Mo) at 65 ^oC in refluxing methanol.

(**Table 4.10**, entry 2), whereas the oxidation of diphenyl sulfide and benzyl phenyl sulfides (**Table 4.10**, entries 10 and 11) were rather sluggish and DBT being least nucleophilic and a relatively inert sulfide, manifested no sulfoxidation reaction under the optimized condition in water even after 12 h of reaction time. Nevertheless, it was possible to selectively oxidize these substrates, even DBT in presence of each of the developed catalysts by replacing H_2O with methanol as medium of reaction and using a higher amount of catalyst (Mo: MPS ratio of 1:100). The reaction was conducted at a moderately elevated temperature of 65 ^{0}C in case of DBT oxidation in order to enhance the reaction rate (**Table 4.10**, entry 12).

As seen from the data of **Table 4.10** (entries 8 and 9), allylic and vinylic sulfides were chemoselectively oxidized to the corresponding sulfoxide without epoxidation of C=C. Similarly, the alcoholic and benzylic sulfides yielded the targeted sulfoxides without affecting any other functional group transformation (**Table 4.10**, entries 7 and 11) under the standard reaction conditions testifying to the excellent functional group tolerance of the catalysts. It is important to highlight herein that we have also confirmed the feasibility of the protocol for scaled-up synthetic applications by conducting the oxidation of thioanisole at ten-fold scale under the standard reaction conditions (**Table 4.10**, entry 1^e).

Furthermore, the oxidations occurred with high utilization efficiency of hydrogen peroxido [57]. The H_2O_2 efficiency in the oxidations was found to be in the range of 90 - 94% in presence of each of the catalysts **PSMo** and **PAMo**. The mild reaction conditions of the protocol with the requirement of reasonably short reaction time appears to be responsible for the observed high H_2O_2 efficiency. In case of DBT oxidation, relatively higher reaction temperature employed and longer reaction time required perhaps facilitates direct H_2O_2 decomposition leading to considerably lower H_2O_2 efficiency (*ca.* 58%).

4.3.2.2 Recyclability of the catalyst

The catalysts could be effectively regenerated *in situ* for reuse in subsequent cycles of reaction, simply by H_2O_2 treatment of the aqueous extract of the spent reaction mixture after separation of the organic product, followed by addition of a fresh batch of substrate after each catalytic cycle. Recycling experiments were conducted under optimized reaction condition using MPS as model substrate. The

regenerated catalysts could be reused for at least ten reaction cycles with the activity and selectivity remaining nearly unaltered [**Fig. 4.17** and **Table 4.10** (entry 1[d])]. It was also possible to recover the catalysts as solid by addition of acetone to aqueous extract of the spent reaction mixture after replenishing the peroxido. The recovered catalyst could be reused in subsequent cycles of reaction without further conditioning.

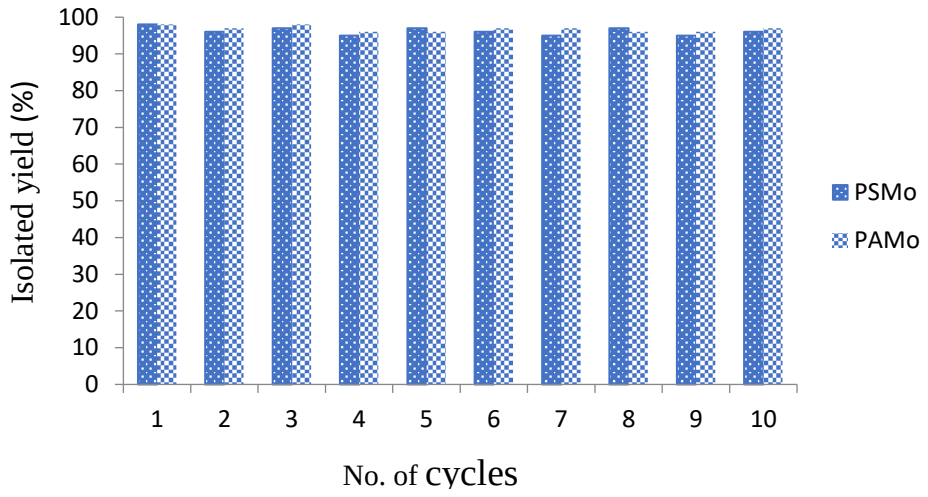

Fig. 4.17 Recyclability of catalyst **PSMo** and **PAMo** for the selective oxidation of sulfide to sulfoxide.

In order to further ascertain the structural integrity of catalysts **PSMo** and **PAMo** during the catalytic cycles, the regenerated catalysts isolated from spent reaction mixture by treatment with acetone, was dried and subsequently subjected to characterization by elemental and spectral analysis. The FTIR spectra of the recovered catalysts showed the signature peaks corresponding to metal-peroxido as well as pendant functional groups of the polymer support as has been observed in the original catalyst (**Fig. 4.18**). Neither the metal loading nor the peroxido content of the recovered catalysts showed any significant decrease compared to the respective starting catalyst as revealed by elemental analysis and EDX spectral data, suggesting that there was no metal leaching out of the polymer during the catalytic process. The ^{95}Mo NMR spectral pattern of the regenerated catalysts was identical with the corresponding spectrum of fresh catalyst (**Fig. 4.19**). Results of our studies thus

confirm that the catalysts are structurally robust being capable of remaining intact during repeated cycle of oxidations.

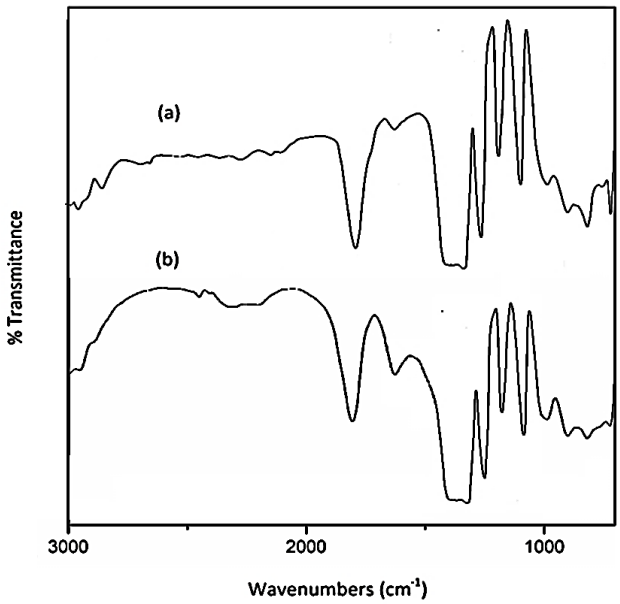

Fig. 4.18 FTIR spectra of (a) **PSMo** and (b) **PSMo** after 10th reaction cycle.

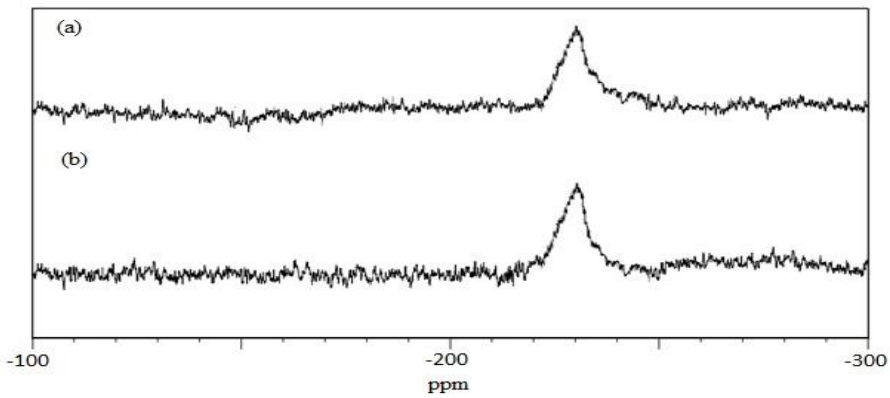

Fig. 4.19 ^{95}Mo NMR spectrum of (a) **PSMo** and (b) **PSMo** after 10th reaction cycle, in D_2O.

4.3.2.3 The proposed catalytic cycle

On the basis of the aforementioned experimental findings, we propose the catalytic cycle for selective oxidation of sulfides to sulfoxide shown in **Fig. 4.20**, using **PSMo** as representative.

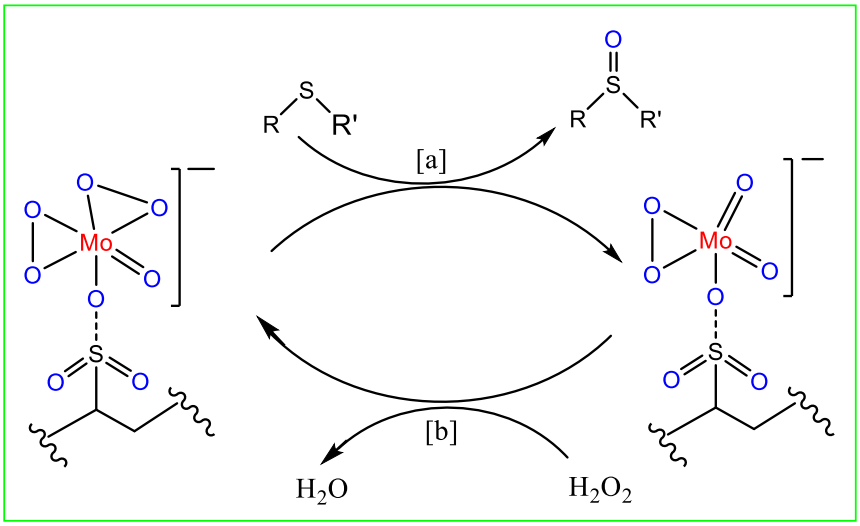

Fig. 4.20 Proposed catalytic cycle.

The first step of the reaction is likely to be the facile transfer of electrophilic oxygen from the active oxidodiperoxidomolybdenum(VI) species of the catalyst to sulfide to afford sulfoxide (reaction a) converting itself into a dioxidomonoperoxido intermediate. The monoperoxido molybdenum derivative eventually combines with H_2O_2 and reverts back to form the original catalyst thus completing the catalytic cycle (reaction b). The proposed reaction cycle is in accord with the previous literature [39,46,101,109-111] on reactivity of **pMo** and peroxidotungsten compounds where the formation of an inactive monoperoxido Mo(VI) and W(IV) intermediate during substrate oxidation by a more reactive diperoxido species of these metals has been well documented.

4.4 Conclusions

In summary, an efficient water tolerant heterogeneous catalyst has been developed by immobilizing peroxidomolybdate moiety in its monoperoxido form on

biopolymer, chitosan which afforded clean conversion of sulfides to the corresponding high purity sulfoxides with 30% H_2O_2 in impressive yield and TOF. On the other hand, diperoxidomolybdenum complexes anchored to linear water-soluble polymers, **PAMo** and **PSMo** served as homogeneous catalysts for selective sulfoxidation in water at room temperature. Under the similar reaction conditions, it was observed that the oxidations proceeded at a homogeneous catalysts (**PAMo** and **PSMo**) exhibited slightly superior catalytic activity over its heterogeneous counterparts as reflected by their respective TOF values. Sustainability of the catalytic strategies have been ensured by the fact that the reactions have been conducted at ambient temperature, using H_2O_2 and water as terminal oxidant and standard green solvent, respectively, avoiding the use of halogenated solvents, co-catalyst or any other types of auxiliaries.

Additional salient features of the catalytic protocols include (i) easy recovery and recyclability with no significant loss in activity or selectivity for several catalytic cycles; (ii) excellent chemoselectivity and ready scalability; (iii) compatibility of both the homogeneous as well as heterogeneous catalytic systems with variety of organic solvents apart from water. Thus our findings demonstrate that linear soluble polymers can be considered as a green and viable alternative to insoluble polymer supports for designing sustainable catalysts for reactions in aqueous medium.

References

1. Wacławek, S., Padil, V. V., and Černík, M. Major advances and challenges in heterogeneous catalysis for environmental applications: a review. *Ecological Chemistry and Engineering S*, 25(1), 9-34, 2018.
2. Piermatti, O., Abu-Reziq, R., and Vaccaro, L. *Catalyst Immobilization: Methods and Applications*. Wiley-VCH, New York, 2019.
3. Sheldon, R.A., Green and sustainable chemistry: challenges and perspectives. *Green Chemistry*, 10:359-360, 2008.
4. Guibal, E. Heterogeneous catalysis on chitosan-based materials: a review. *Progress in Polymer Science*, 30(1):71-109, 2005.
5. Rinaudo, M. Chitin and chitosan: properties and applications. *Progress in Polymer science*, 31(7):603-632, 2006.
6. Macquarrie, D. J. and Hardy, J. J. Applications of functionalized chitosan in catalysis. *Industrial & Engineering Chemistry Research*, 44(23):8499-8520, 2005.
7. Hamed, I., Özogul, F., and Regenstein, J. M. Industrial applications of crustacean by-products (chitin, chitosan, and chitooligosaccharides): A review. *Trends in Food Science & Technology*, 48:40-50, 2016.
8. Kumar, M. N. R. A review of chitin and chitosan applications. *Reactive and Functional Polymers*, 46(1):1-27, 2000.
9. Lee, M., Chen, B. Y., and Den, W. Chitosan as a natural polymer for heterogeneous catalysts support: a short review on its applications. *Applied Sciences*, 5(4):1272-1283, 2015.
10. Rashid, S., Shen, C., Yang, J., Liu, J., and Li, J. Preparation and properties of chitosan–metal complex: some factors influencing the adsorption capacity for dyes in aqueous solution. *Journal of Environmental Sciences*, 66:301-309, 2018.
11. Liu, W., Qin, Y., Liu, S., Xing, R., Yu, H., Chen, X., Li, K., and Li, P. C-coordinated O-carboxymethyl chitosan metal complexes: Synthesis, characterization and antifungal efficacy. *International Journal of Biological Macromolecules*, 106:68-77, 2018.
12. Gerente, C., Lee, V. K. C., Cloirec, P. L., and McKay, G. Application of chitosan for the removal of metals from wastewaters by adsorption—mechanisms and models review. *Critical Reviews in Environmental Science and Technology*, 37(1): 41-127, 2007.
13. Dash, M., Chiellini, F., Ottenbrite, R. M., and Chiellini, E. Chitosan—A versatile semi-synthetic polymer in biomedical applications. *Progress in Polymer Science*, 36(8):981-1014, 2011.

14. Varma, A. J., Deshpande, S. V., and Kennedy, J. F. Metal complexation by chitosan and its derivatives: a review. *Carbohydrate Polymers*, 55(1):77-93, 2004.
15. Zhou, J., Dong, Z., Yang, H., Shi, Z., Zhou, X., and Li, R. Pd immobilized on magnetic chitosan as a heterogeneous catalyst for acetalization and hydrogenation reactions. *Applied Surface Science*, 279:360-366, 2013.
16. Ma, L., Su, Y., Chen, J., and Xu, J. Silica/Chitosan core–shell hybrid-microsphere-supported Pd catalyst for hydrogenation of cyclohexene reaction. *Industrial & Engineering Chemistry Research*, 56(44):12655-12662, 2017.
17. Baran, T., Açıksöz, E., and Menteş, A. Highly efficient, quick and green synthesis of biarlys with chitosan supported catalyst using microwave irradiation in the absence of solvent. *Carbohydrate Polymers*, 142:189-198, 2016.
18. Franconetti, A., Domínguez-Rodríguez, P., Lara-García, D., Prado-Gotor, R., and Cabrera-Escribano, F. Native and modified chitosan-based hydrogels as green heterogeneous organocatalysts for imine-mediated Knoevenagel condensation. *Applied Catalysis A: General*, 517:176-186, 2016.
19. Adlim, M., Bakar, M. A., Liew, K. Y., and Ismail, J. Synthesis of chitosan-stabilized platinum and palladium nanoparticles and their hydrogenation activity. *Journal of Molecular Catalysis A: Chemical*, 212(1-2):141-149, 2004.
20. Tanioka, A., Shimizu, K., Hosono, T., Eto, R., and Osaki, T. Effect of interfacial state in bipolar membrane on rectification and water splitting. *Colloids and Surfaces A: Physicochemical and Engineering Aspects*, 159(2-3):395-404, 1999.
21. Rajesh, A. M., Kumar, M., and Shahi, V. K. Functionalized biopolymer based bipolar membrane with poly ethylene glycol interfacial layer for improved water splitting. *Journal of Membrane Science*, 372(1-2):249-257, 2011.
22. Yi, S. S., Lee, D. H., Sin, E., and Lee, Y. S. Chitosan-supported palladium (0) catalyst for microwave-prompted Suzuki cross-coupling reaction in water. *Tetrahedron Letters*, 48(38):6771-6775, 2007.
23. Veisi, H., Najafi, S., and Hemmati, S. Pd (II)/Pd (0) anchored to magnetic nanoparticles (Fe_3O_4) modified with biguanidine-chitosan polymer as a novel nanocatalyst for Suzuki-Miyaura coupling reactions. *International Journal of Biological Macromolecules*, 113:186-194, 2018.
24. kaur, P., Kumar, B., Kumar, V., and Kumar, R. Chitosan-supported copper as an efficient and recyclable heterogeneous catalyst for A3/decarboxylative A3-coupling reaction. *Tetrahedron Letters*, 59(21):1986-1991, 2018.
25. Huai-min, G. and Xian-su, C. Study of cobalt (II)-chitosan coordination polymer and its catalytic activity and selectivity for vinyl monomer polymerization. *Polymers for Advanced Technologies*, 15(1-2):89-92, 2004.

26. Inaki, Y., Otsuru, M., and Takemoto, K. Vinyl polymerization by metal complexes. XXXI. Initiation by chitosan-copper(II) complex. *Journal of Macromolecular Science: Part A-Chemistry*, 12(7):953-970, 1978.
27. Huang, K., Liu, H. W., Dou, X., Huang, M. Y., and Jiang, Y. Y. Silica-supported chitosan–osmium tetroxide complex catalyzed vicinal hydroxylation of olefins using hexacyanoferrate(III) ion as a cooxidant. *Polymers for Advanced Technologies*, 14(3-5):366-370, 2003.
28. Xue, L., Zhou, D. J., Tang, L., Ji, X. F., Huang, M. Y., and Jiang, Y. Y. The asymmetric hydration of 1-octene to (S)-(+)-2-octanol with a biopolymer–metal complex, silica-supported chitosan–cobalt complex. *Reactive and Functional Polymers*, 58(2):117-121, 2004.
29. Hardy, J. J., Hubert, S., Macquarrie, D. J., and Wilson, A. J. Chitosan-based heterogeneous catalysts for Suzuki and Heck reactions. *Green Chemistry*, 6(1):53-56, 2004.
30. Calò, V., Nacci, A., Monopoli, A., Fornaro, A., Sabbatini, L., Cioffi, N., and Ditaranto, N. Heck reaction catalyzed by nanosized palladium on chitosan in ionic liquids. *Organometallics*, 23(22): 5154-5158, 2004.
31. Makhubela, B. C., Jardine, A., and Smith, G. S. Pd nanosized particles supported on chitosan and 6-deoxy-6-amino chitosan as recyclable catalysts for Suzuki–Miyaura and Heck cross-coupling reactions. *Applied Catalysis A: General*, 393(1-2):231-241, 2011.
32. Kumari, S., Layek, S., and Pathak, D. D. Palladium nanoparticles immobilized on a magnetic chitosan-anchored Schiff base: applications in Suzuki–Miyaura and Heck–Mizoroki coupling reactions. *New Journal of Chemistry*, 41(13):5595-5604, 2017.
33. Baran, T. and Menteş, A. Highly efficient Suzuki cross-coupling reaction of biomaterial supported catalyst derived from glyoxal and chitosan. *Journal of Organometallic Chemistry*, 803:30-38, 2016.
34. Zhu, J., Wang, P. C., and Lu, M. Synthesis of novel magnetic chitosan supported protonated peroxotungstate and its catalytic performance for oxidation. *New Journal of Chemistry*, 36(12): 2587-2592, 2012.
35. Zhu, J., Zhao, X. J., Wang, P. C., and Lu, M. Green oxidation process in the synthesis of LLM-105 with H_2O_2/peroxotungstate system and its theoretical study. *Journal of Heterocyclic Chemistry*, 53(5):1386-1394, 2016.
36. Zhao, G., Tan, R., Zhang, Y., Luo, X., Xing, C., and Yin, D. Cooperative chiral salen Ti IV catalysts with built-in phase-transfer capability accelerate asymmetric sulfoxidation in water. *RSC Advances*, 6(29):24704-24711, 2016.

37. Rayati, S. and Nejabat, F. Catalytic activity of Fe-porphyrins grafted on multiwalled carbon nanotubes in the heterogeneous oxidation of sulfides and degradation of phenols in water. *ComptesRendusChimie*, 20(9-10):967-974, 2017.
38. Aghajani, M., Safaei, E., and Karimi, B. Selective and green oxidation of sulfides in water using a new iron (III) bis (phenol) amine complex supported on functionalized graphene oxide. *Synthetic Metals*, 233:63-73, 2017.
39. Choudary, B. M., Bharathi, B., Reddy, C. V., and Kantam, M. L. Tungstate-exchanged Mg-Al-LDH catalyst: an eco-compatible route for the oxidation of sulfides in aqueous medium. *Journal of the Chemical Society, Perkin Transactions* 1(18):2069-2074, 2002.
40. Prasanth, K. L. and Maheswaran, H. Selective oxidation of sulfides to sulfoxides in water using 30% hydrogen peroxide catalyzed with a recoverable $VO(acac)_2$ exchanged sulfonic acid resin catalyst. *Journal of Molecular Catalysis A: Chemical*, 268(1-2):45-49, 2007.
41. Rajabi, F., Naserian, S., Primo, A., and Luque, R. Efficient and highly selective aqueous oxidation of sulfides to sulfoxides at room temperature catalysed by supported iron oxide nanoparticles on SBA-15. *Advanced Synthesis & Catalysis*, 353(11-12):2060-2066, 2011.
42. Egami, H. and Katsuki, T. Fe (salan)-catalyzed asymmetric oxidation of sulfides with hydrogen peroxide in water. *Journal of the American Chemical Society*, 129(29):8940-8941, 2007.
43. Zeng, X. M., Chen, J. M., Yoshimura, A., Middleton, K., and Zhdankin, V. V. SiO_2-supported RuCl 3/3-(dichloroiodo) benzoic acid: green catalytic system for the oxidation of alcohols and sulfides in water. *RSC Advances*, 1(6):973-977, 2011.
44. Maurya, M. R., Arya, A., Kumar, A., Kuznetsov, M. L., Avecilla, F., and Costa Pessoa, J. Polymer-bound oxidovanadium(IV) and dioxidovanadium(V) complexes as catalysts for the oxidative desulfurization of model fuel diesel. *Inorganic Chemistry*, 49(14):6586-6600, 2010.
45. Choudary, B. M., Bharathi, B., Reddy, C. V., and Kantam, M. L. Tungstate-exchanged Mg-Al-LDH catalyst: an eco-compatible route for the oxidation of sulfides in aqueous medium. *Journal of the Chemical Society, Perkin Transactions*, 1(18):2069-2074, 2002.
46. Boruah, J. J., Das, S. P., Ankireddy, S. R., Gogoi, S. R., and Islam, N. S. Merrifield resin supported peroxomolybdenum (VI) compounds: recoverable heterogeneous catalysts for the efficient, selective and mild oxidation of organic sulfides with H_2O_2. *Green Chemistry*, 15(10):2944-2959, 2013.

47. Gogoi, S. R., Boruah, J. J., Sengupta, G., Saikia, G., Ahmed, K., Bania, K. K., and Islam, N. S. Peroxoniobium(V)-catalyzed selective oxidation of sulfides with hydrogen peroxide in water: a sustainable approach. *Catalysis Science & Technology*, 5(1):595-610, 2015.
48. Karmee, S. K., Greiner, L., Kraynov, A., Müller, T. E., Niemeijer, B., and Leitner, W. Nanoparticle catalysed oxidation of sulfides to sulfones by in situ generated H_2O_2 in supercritical carbon dioxide/water biphasic medium. *Chemical Communications*, 46(36):6705-6707, 2010.
49. Conte, V. and Floris, B. Vanadium and molybdenum peroxides: synthesis and catalytic activity in oxidation reactions. *Dalton Transactions*, 40(7):1419-1436, 2011.
50. Hussain, S., Talukdar, D., Bharadwaj, S. K., and Chaudhuri, M. K. $VO_2F(dmpz)_2$: a new catalyst for selective oxidation of organic sulfides to sulfoxides with H_2O_2. *Tetrahedron Letters*, 53(48): 6512-6515, 2012.
51. Romanelli, G. P., Villabrille, P. I., Cáceres, C. V., Vázquez, P. G., and Tundo, P. Keggin heteropolycompounds as catalysts for liquid-phase oxidation of sulfides to sulfoxides/sulfones by hydrogen peroxide. *Catalysis Communications*, 12(8):726-730, 2011.
52. Bagherzadeh, M., Latifi, R., Tahsini, L., and Amini, M. Catalytic oxidation of sulfides to sulfoxide using manganese (III) complexes with bidentate O, N-donor oxazoline ligand and UHP oxidizing agent. *Catalysis Communications*, 10(2):196-200, 2008.
53. Egami, H. and Katsuki, T. Fe (salan)-catalyzed asymmetric oxidation of sulfides with hydrogen peroxide in water. *Journal of the American Chemical Society*, 129(29):8940-8941, 2007.
54. Yang, C., Jin, Q., Zhang, H., Liao, J., Zhu, J., Yu, B., and Deng, J. Tetra-(tetraalkylammonium) octamolybdate catalysts for selective oxidation of sulfides to sulfoxides with hydrogen peroxide. *Green Chemistry*, 11(9):1401-1405, 2009.
55. Kamata, K., Hirano, T., and Mizuno, N. Highly efficient oxidation of sulfides with hydrogen peroxide catalyzed by $[SeO_4\{WO(O_2)_2\}_2]_2-$. *Chemical Communications*, (26):3958-3960, 2009.
56. Sato, K., Hyodo, M., Aoki, M., Zheng, X. Q., and Noyori, R. Oxidation of sulfides to sulfoxides and sulfones with 30% hydrogen peroxide under organic solvent-and halogen-free conditions. *Tetrahedron*, 57(13):2469-2476, 2001.
57. Hulea, V., Maciuca, A. L., Fajula, F., and Dumitriu, E. Catalytic oxidation of thiophenes and thioethers with hydrogen peroxide in the presence of W-containing layered double hydroxides. *Applied Catalysis A: General*, 313(2):200-207, 2006..

58. Boruah, J. J., Kalita, D., Das, S. P., Paul, S., and Islam, N. S. Polymer-anchored peroxo compounds of vanadium (V) and molybdenum (VI): synthesis, stability, and their activities with alkaline phosphatase and catalase. *Inorganic Chemistry*, 50(17):8046-8062, 2011.
59. Boruah, J. J., Ahmed, K., Das, S., Gogoi, S. R., Saikia, G., Sharma, M., and Islam, N. S. Peroxomolybdate supported on water soluble polymers as efficient catalysts for green and selective sulfoxidation in aqueous medium. *Journal of Molecular Catalysis A: Chemical*, 425:21-30, 2016.
60. Delley, B. From molecules to solids with the DMol 3 approach. *The Journal of Chemical Physics*, 113(18):7756-7764, 2000.
61. Appalakondaiah, S., Vaitheeswaran, G., Lebegue, S., Christensen, N. E., and Svane, A. Effect of van der Waals interactions on the structural and elastic properties of black phosphorus. *Physical Review B*, 86(3):035105, 2012.
62. Vosko, S. H., Wilk, L., and Nusair, M. Accurate spin-dependent electron liquid correlation energies for local spin density calculations: a critical analysis. *Canadian Journal of Physics*, 58(8):1200-1211, 1980.
63. Ortmann, F., Bechstedt, F., and Schmidt, W. G. Semiempirical van der Waals correction to the density functional description of solids and molecular structures. *Physical Review B*, 73(20):205101, 2006.
64. Zhou, J., Xiao, F., Wang, W.N., and Fan, K. N. Theoretical study of the interaction of nitric oxide with small neutral and charged silver clusters. *Journal of Molecular Structure: THEOCHEM*, 818(1-3):51-55, 2007.
65. Delley, B. A scattering theoretic approach to scalar relativistic corrections on bonding. *International Journal of Quantum Chemistry*, 69(3):.423-433, 1998.
66. Trimukhe, K. D. and Varma, A. J. A morphological study of heavy metal complexes of chitosan and crosslinked chitosans by SEM and WAXRD. *Carbohydrate Polymers*, 71(4):698-702, 2008.
67. Roosen, J., Spooren, J., and Binnemans, K. Adsorption performance of functionalized chitosan–silica hybrid materials toward rare earths. *Journal of Materials Chemistry A*, 2(45):19415-19426, 2014.
68. Hussein, M. H. M., El-Hady, M. F., Sayed, W. M., and Hefni, H. Preparation of some chitosan heavy metal complexes and study of its properties. *Polymer Science Series A*, 54(2):113-124, 2012.
69. Hu, Q., Chen, N., Feng, C., Hu, W., Zhang, J., Liu, H., and He, Q. Nitrate removal from aqueous solution using granular chitosan-Fe (III)–Al (III) complex: kinetic, isotherm and regeneration studies. *Journal of the Taiwan Institute of Chemical Engineers*, 63:216-225, 2016.

70. Webster, A., Halling, M. D., and Grant, D. M. Metal complexation of chitosan and its glutaraldehyde cross-linked derivative. *Carbohydrate Research*, 342(9):1189-1201, 2007.
71. Acharyulu, S. R., Gomathi, T., and Sudha, P. N. Physico-chemical characterization of cross linked chitosan-polyacrylonitrile polymer blends. *Der Pharmacia Lettre*, 5(2):354-363, 2013.
72. Brunauer, S., Emmett, P. H., and Teller, E. Adsorption of gases in multimolecular layers. *Journal of the American Chemical Society*, 60(2):309-319, 1938.
73. Barrett, E. P., Joyner, L. G., and Halenda, P. P. The determination of pore volume and area distributions in porous substances. I. Computations from nitrogen isotherms. *Journal of the American Chemical Society*, 73(1):373-380, 1951.
74. Sing, K. S., Everett, D. H., Haul, R. A. W., Moscou, L., Pierotti, R. A., Rouquerol, J., and Siemieniewska, T. International union of pure commission on colloid and surface chemistry including catalysis* reporting physisorption data for gas/solid systems with special reference to the determination of surface area and porosity. *Pure Applied Chemistry*, 57(4):603-619, 1985.
75. Gregg, S. J. and Sing, K. S. W. *Adsorption, Surface Area and Porosity*, Academic Press, London, 1982.
76. Hernández, R. B., Franco, A. P., Yola, O. R., Lopez-Delgado, A., Felcman, J., Recio, M. A. L., and Mercê, A. L. R. Coordination study of chitosan and Fe^{3+}. *Journal of Molecular Structure*, 877(1-3):89-99, 2008.
77. Pornsunthorntawee, O., Katepetch, C., Vanichvattanadecha, C., Saito, N., and Rujiravanit, R. Depolymerization of chitosan–metal complexes via a solution plasma technique. *Carbohydrate Polymers*, 102:504-512, 2014.
78. Antony, R., David, S. T., Saravanan, K., Karuppasamy, K., and Balakumar, S. Synthesis, spectrochemical characterization and catalytic activity of transition metal complexes derived from Schiff base modified chitosan. *Spectrochimica Acta Part A: Molecular and Biomolecular Spectroscopy*, 103:423-430, 2013.
79. Wang, X., Du, Y., and Liu, H. Preparation, characterization and antimicrobial activity of chitosan–Zn complex. *Carbohydrate Polymers*, 56(1):21-26, 2004.
80. Baran, T. and Menteş, A. Polymeric material prepared from Schiff base based on O-carboxymethyl chitosan and its Cu(II) and Pd(II) complexes. *Journal of Molecular Structure*, 1115:220-227, 2016.
81. Tang, L. G. and Hon, D. N. S. Chelation of chitosan derivatives with zinc ions. II. Association complexes of Zn^{2+} onto O, N-carboxymethyl chitosan. *Journal of Applied Polymer Science*, 79(8):1476-1485, 2001.

82. Piron, E. and Domard, A. Interaction between chitosan and uranyl ions. Part 2. Mechanism of interaction. *International Journal of Biological Macromolecules*, 22(1):33-40, 1998.
83. Mekahlia, S. and Bouzid, B. Chitosan-Coppe(II) complex as antibacterial agent: synthesis, characterization and coordinating bond-activity correlation study. *Physics Procedia*, 2(3):1045-1053, 2009.
84. Kramareva, N. V., Stakheev, A. Y., Tkachenko, O. P., Klementiev, K. V., Grünert, W., Finashina, E. D., and Kustov, L. M. Heterogenized palladium chitosan complexes as potential catalysts in oxidation reactions: study of the structure. *Journal of Molecular Catalysis A: Chemical*, 209(1-2):97-106, 2004
85. Campbell, N. J., Dengel, A. C., and Griffith, W. P. Studies on transition metal peroxo complexes—X. The nature of peroxovanadates in aqueous solution. *Polyhedron*, 8(11):1379-1386, 1989.
86. Lever, A. B. P. and Gray, H. B. Electronic spectra of metal-dioxygen complexes. *Accounts of Chemical Research*, 11(9):348-355, 1978.
87. Dengel, A. C., Griffith, W. P., Powell, R. D., and Skapski, A. C. X-Ray structure of $K_4[Mo_2O_2(O_2)_4(C_4H_2O_6)]\cdot 4H_2O$, a novel peroxo complex containing a single tetradentate bridging tartrate. *Journal of the Chemical Society, Chemical Communications*, (7):555-556, 1986.
88. Djordjevic, C., Puryear, B. C., Vuletic, N., Abelt, C. J., and Sheffield, S. J. Preparation, spectroscopic properties, and characterization of novel peroxo complexes of vanadium(V) and molybdenum(VI) with nicotinic acid and nicotinic acid N-oxide. *Inorganic Chemistry*, 27(17):2926-2932, 1988.
89. Maurya, M. R. and Bharti, N. Synthesis, thermal and spectral studies of oxoperoxo and dioxo complexes of vanadium (V), molybdenum (VI) and tungsten (VI) with 2-(α-hydroxyalkyl/aryl) benzimidazole. *Transition Metal Chemistry*, 24(4):389-393, 1999.
90. Guibal, E., Milot, C., Eterradossi, O., Gauffier, C., and Domard, A. Study of molybdate ion sorption on chitosan gel beads by different spectrometric analyses. *International Journal of Biological Macromolecules*, 24(1):49-59, 1999.
91. Prashanth, K. H., Kittur, F. S., and Tharanathan, R. N. Solid state structure of chitosan prepared under different N-deacetylating conditions. *Carbohydrate Polymers*, 50(1):27-33, 2002.
92. Saito, H., Tabeta, R., and Ogawa, K. High-resolution solid-state carbon-13 NMR study of chitosan and its salts with acids: conformational characterization of polymorphs and helical structures as viewed from the conformation-dependent carbon-13 chemical shifts. *Macromolecules*, 20(10):2424-2430, 1987.

93. Trimukhe, K. D. and Varma, A. J. Metal complexes of crosslinked chitosans: Correlations between metal ion complexation values and thermal properties. *Carbohydrate Polymers*, 75(1):63-70, 2009.
94. Dengel, A. C., Griffith, W. P., Powell, R. D., and Skapski, A. C. Studies on transition-metal peroxo complexes. Part 7. Molybdenum (VI) and tungsten (VI) carboxylato peroxo complexes, and the X-ray crystal structure of $K_2[MoO(O_2)_2(glyc)]\cdot 2H_2O$. *Journal of the Chemical Society, Dalton Transactions*, (5):991-995, 1987.
95. Paul, S. S., Selim, M., and Mukherjea, K. K. Synthesis, characterization and DNA nuclease activity of oxo-peroxomolybdenum (VI) complexes. *Journal of Coordination Chemistry*, 70(10): 1739-1760, 2017.
96. Bonchio, M., Conte, V., Assunta De Conciliis, M., Di Furia, F., Ballistreri, F. P., Tomaselli, G. A., and Toscano, R. M. The Relative Reactivity of Thioethers and Sulfoxides toward Oxygen Transfer Reagents: The Oxidation of Thianthrene 5-Oxide and Related Compounds by MoO_5HMPT. *The Journal of Organic Chemistry*, 60(14):4475-4480, 1995.
97. Maciuca, A. L., Ciocan, C. E., Dumitriu, E., Fajula, F., and Hulea, V. V-, Mo-and W-containing layered double hydroxides as effective catalysts for mild oxidation of thioethers and thiophenes with H_2O_2. *Catalysis Today*, 138(1-2):33-37, 2008.
98. Kholdeeva, O. A. Hydrogen Peroxide Activation over TiIV: What Have We Learned from Studies on Ti-Containing Polyoxometalates?. *European Journal of Inorganic Chemistry*, 2013(10-11):1595-1605, 2013.
99. Bortolini, O., Di Furia, F., Modena, G., and Seraglia, R. Metal catalysis in oxidation by peroxides. Sulfide oxidation and olefin epoxidation by dilute hydrogen peroxide, catalyzed by molybdenum and tungsten derivatives under phase-transfer conditions. *The Journal of Organic Chemistry*, 50(15):2688-2690, 1985.
100. Das, S. P., Boruah, J. J., Sharma, N., and Islam, N. S. New polymer-immobilized peroxotungsten compound as an efficient catalyst for selective and mild oxidation of sulfides by hydrogen peroxide. *Journal of Molecular Catalysis A: Chemical*, 356:36-45, 2012.
101. Das, S. P., Boruah, J. J., Chetry, H., and Islam, N. S. Selective oxidation of organic sulfides by mononuclear and dinuclearperoxotungsten(VI) complexes. *Tetrahedron Letters*, 53(9):1163-1168, 2012.
102. Ghiron, A. F. and Thompson, R. C. Comparative kinetic study of oxygen atom transfer reactions of oxohydroxodiperoxomolybdenum(VI) and oxo (oxalato)

diperoxomolybdenum(VI) in aqueous solution. *Inorganic Chemistry*, 28(19):3647-3650, 1989.

103. Reynolds, M. S., Morandi, S. J., Raebiger, J. W., Melican, S. P., and Smith, S. P. Kinetics of bromide oxidation by (oxalato) oxodiperoxomolybdate(VI). *Inorganic Chemistry*, 33(22):4977-4984, 1994.
104. Sensato, F. R., Custodio, R., Longo, E., Safont, V. S., and Andres, J. Sulfide and sulfoxide oxidations by mono-and diperoxo complexes of molybdenum. A density functional study. *The Journal of Organic Chemistry*, 68(15):5870-5874, 2003.
105. Djordjevic, C., Vuletic, N., and Sinn, E. Synthesis and properties of peroxo α-amino acid complexes of molybdenum (VI). The structures of $MoO(O_2)_2(HAA)(H_2O)$, HAA= glycine, proline. *Inorganica Chimica Acta*, 104(1):L7-L9, 1985.
106. Gharah, N., Chakraborty, S., Mukherjee, A. K., and Bhattacharyya, R. Oxoperoxo molybdenum(VI)-and tungsten(VI) complexes with 1-(2′-hydroxyphenyl) ethanone oxime: Synthesis, structure and catalytic uses in the oxidation of olefins, alcohols, sulfides and amines using H_2O_2 as a terminal oxidant. *Inorganica Chimica Acta*, 362(4):1089-1100, 2009.
107. Kalita, D., Das, S. P., and Islam, N. S. Kinetics of inhibition of rabbit intestine alkaline phosphatase by heteroligand peroxo complexes of vanadium(V) and tungsten(VI). *Biological Trace Element Research*, 128(3):200-219, 2009.
108. Hazarika, P., Kalita, D., Sarmah, S., Borah, R., and Islam, N. S. New oxo-bridged dinuclearperoxotungsten(VI) complexes: Synthesis, stability and activity in bromoperoxidation. *Polyhedron*, 25(18):3501-3508, 2006.
109. Mimoun, H. Do metal peroxides as homolytic and heterolytic oxidative reagents. Mechanism of the halcon epoxidation process. *Catalysis Today*, 1(3):281-295, 1987.
110. Jørgensen, K. A. Transition-metal-catalyzed epoxidations. *Chemical Reviews*, 89(3):431-4581989.
111. Thiel, W. R. and Eppinger, J. Molybdenum-Catalyzed Olefin Epoxidation: Ligand Effects. *Chemistry–A European Journal*, 3(5):696-705, 1997.